The Dissertation Committee for Orrin Abraham Shindell certifies that this is the approved version of the following dissertation:

Pattern Formation in Cell-Sized Membranes

Committee:

Vernita Gordon, Supervisor

Ernst-Ludwig Florin

Michael Marder

Jeanne Stachowiak

Roger Bonnecaze

Pattern Formation in Cell-Sized Membranes

by

Orrin Abraham Shindell, B.S.

Dissertation
Presented to the Faculty of the Graduate School of
The University of Texas at Austin
in Partial Fulfillment
of the Requirements
for the degree of
Doctor of Philosophy

The University of Texas at Austin
May, 2017

To Vanessa Gelvin for support and inspiration.

Pattern Formation in Cell-Sized Membranes

Publication No. _____

Orrin Abraham Shindell, Ph.D.
The University of Texas at Austin, 2017

Supervisor: Vernita Gordon

The research presented in this dissertation follows in the tradition of experimental membrane biophysics. Our goal is to study the physical mechanisms underlying organization in the plasma membrane of living cells by using model systems. The central result from our experiments is that mixed-lipid membrane vesicles that are adhered by proteins to a solid-supported lipid membrane can dynamically form long-lived holes at the adhesion interface between the membranes.

The first set of experiments we discuss exhibit the stable persistence of static patterns. The patterns are formed by adhering ternary-lipid vesicle membranes to a planar membrane supported on a solid, glass substrate *via* biotin-avidin binding. The membrane and avidin are marked with spectrally distinct fluorescent dyes. We use fluorescence microscopy to acquire data. Adhesion causes half of adhered vesicles to form rough annular patterns with a central region that is devoid of membrane dye and protein binders. The peripheral region is dense in proteins and enriched in dye compared to the free, non-adhered portion of the same membrane. We measure the volume V and surface area A of adhered membranes. Using the measure $6\sqrt{\pi}V/A^{3/2}$ we find 0.84 for patterned and 0.98 for non-patterned membranes. Thus, adhered vesicles have two equilibrium states, one with annular patterns and one without, and the transition between them involves a loss of internal volume. Collectively our results suggest the annular patterns are holes.

Finally, we report on a dynamic pattern that occurs in binary-lipid membranes adhered to a supported lipid bilayer. The pattern consists of finger-shaped holes that invade the protein-bound region. We show the characteristics of the fingers depend on

the density ρ of the protein binders in the adhered region: the width of static fingers λ scales as $\lambda \sim \rho$ and the rate of finger formation r, defined as the number of fingers that branch off from a boundary per unit time, scales as $\ln r \sim \rho$. Theoretically, we treat the formation of a finger as a thermally activated event occurring in a tense elastic film. The activation energy required to form a finger is ≈ 3.5 kT, a biologically relevant energy scale.

Contents

List of Figures

Chapter One: Overview of Author's Contributions

This dissertation is based on two published peer-reviewed articles and one manuscript being currently developed into a research article for submission. Those two articles and manuscript, along with another article with which this author was involved, are listed below. This author's contributions to each is briefly discussed.

1.0.1 Published Works

[1] Vernita D Gordon, TJ O'Halloran, and O Shindell. Membrane adhesion and the formation of heterogeneities: biology, biophysics, and biotechnology. Physical Chemistry Chemical Physics, 17(24):15522–15533, 2015.

This article is an invited review published in a special topics edition of Physical Chemistry Chemical Physics: **Chemical compartmentalisation by membranes: from biological mechanism to biomimetic applications**. The article was composed of three major parts, biology, biophysics, and biotechnology. This author's primary contribution to the review was to conduct a literature search and write the section on biophysics, which dealt primarily with reviewing membrane adhesion and membrane phase separation experiments. The article comprises Chapter 2 of this dissertation and serves the purpose of an introduction to membrane biophysics.

[2] O Shindell, N Mica, M Ritzer, and Vernita D Gordon. Specific adhesion of membranes simultaneously supports dual heterogeneities in lipids and proteins. Physical Chemistry Chemical Physics, 17(24):15598–15607, 2015. 2, 15

This article, which forms the third chapter of this dissertation, is a research article also published in the special topics edition of Physical Chemistry Chemical Physics: **Chemical compartmentalisation by membranes: from biological mechanism to biomimetic applications**. The article presented the results from a series of experiments that were done by adhering with proteins multicomponent lipid membrane vesicles to a flat supported lipid membrane. The central result was that this

system was capable of stabilizing heterogenous annular patterns at the adhesion site between the two membranes. There was, at the time of publication, some confusion about the physical mechanisms that gave rise to the formation of the observed patterns. In retrospect, the confusion was warranted because it appears now that the pattern probably was not of the nature the authors thought.

Briefly, mixed-lipid membranes are capable of separating into coexisting phases. The standard experimental method for determining the coexistence of lipid phases is to incorporate a fluorescent membrane dye into the membrane, which preferentially partitions away from one phase. Thus, one phase appears bright and the other phase appears dark in a fluorescence microscope. The annular patterns had this signature: a central region devoid of membrane dye, and a peripheral region concentrated in membrane dye. Furthermore, the separation of lipid phases at the adhesion site between the two membranes was expected for theoretical reasons. Despite the experimental evidence and theoretical prediction, the central region appears not to have been a lipid phase at all, rather it now appears to have been a hole in the membrane. This result had the same experimental readout as lipid phase separation but lacked any existing theoretical justification. Hence, the authors were misled.

The fourth chapter of this dissertation, discussed more below, is based on a different set of experiments that brought to light the mistake the authors had made. Fortunately, the results of those experiments and the theoretical modeling accompanying them, give a more complete and accurate picture of the experimental results presented in the article *Specific adhesion of membranes simultaneously supports dual heterogeneities in lipids and proteins* and Chapter 3 of this dissertation. Of the two possible explanations for the formation of the annular patterns put forth in the article *Specific adhesion of membranes simultaneously supports dual heterogeneities in lipids and proteins*, the second was more consistent with our later observations.

The contribution of this author to the article *Specific adhesion of membranes simultaneously supports dual heterogeneities in lipids and proteins* was to develop the experiments, take and analyze the data, generate the figures, and write the paper. Furthermore, two undergraduate students, who are the second and third authors, worked closely with this author in the lab and learned to do experimental and analytical work. Both have gone on to pursue higher degrees, one in physics (Natalie Mica) and one in medicine (Max Ritzer).

[3] O Shindell, N. Mica, and Vernita D. Gordon. On a Nonequilibrium Fingering Pattern in Adhered Lipid Membranes. (Manuscript In Preparation)

Chapter 4 is based on a manuscript in preparation that unifies, in some degree, the previous work. The central experimental result is that multicomponent lipid membranes that *do not* undergo phase separation, i.e., that are miscible at all temperatures, can form dynamic fingering patterns when they are adhered to a supported membrane. The characteristics of the growing fingers depend on the binding protein density in two ways: as the density increases the width of the fingers that form decreases and the rate at which new fingers form decreases. It is shown, that these observations are consistent with a free energy function that is based on the thermal theory of tension-induced pore formation.

The contributions of this author to the manuscript were to develop the experiments, take and analyze the data, generate the figures, develop the theory, and write the manuscript.

[4] Karishma S Kaushik, Jake Stolhandske, Orrin Shindell, Hugh D Smyth, and Vernita D Gordon. Tobramycin and bicarbonate synergise to kill planktonic pseudomonas aeruginosa, but antagonise to promote biofilm survival. npj Biofilms and Microbiomes, 2:16006, 2016. 4

This article does not occupy a formal place in the dissertation, though it does in the author's doctoral work. This author's contribution was to work with the undergraduate student Jake Stolhandske on computer analysis of experimental data. The student had an idea for a way to model the data, which was published in the paper, and wanted to used Matlab to employ it. The author taught the student some Matlab basics and helped to employ the model.

Chapter Two: Membrane adhesion and the formation of heterogeneities: biology, biophysics, and biotechnology

Membrane adhesion is essential to many vital biological processes. Sites of membrane adhesion are often associated with heterogeneities in the lipid and protein composition of the membrane. These heterogeneities are thought to play functional roles by facilitating interactions between proteins. However, the causal links between membrane adhesion and membrane heterogeneities are not known. Here we survey the state of the field and indicate what we think are understudied areas ripe for development.

2.1 Introduction

The close approach and subsequent adherence and fusion of one membrane with another is a frequent event that underlies the organization of all eukaryotic cells. Membrane adhesion can be found in structures that range in scale from the entire plasma membrane of a 50 micron cell as it adheres to a substratum to an individual 50 nm secretory vesicle that adheres to a target organelle in the cell interior. The past decade has led to an increasing understanding of the heterogeneous arrangement of lipids and proteins in membranes. Less frequently considered is how membrane adhesion and heterogeneity influence each other. Consideration of this interplay can lead to new mechanistic insights in how cell membranes function and also aid the design of lipid carriers for delivery of therapeutics.

This Chapter is based on a review article that considers how membrane adhesion and membrane heterogeneity interact. We begin by highlighting cellular events where membrane adhesion and heterogeneity are key factors in cellular functions. We then consider how these events are studied in experimental model membranes where the components can be defined. Finally while both the specific adhesion of lipid membranes to targets and the formation of lateral heterogeneities in membranes have been advanced as means of making "smarter" more responsive membrane-based therapeutics, to our knowledge these two streams of investigation have not yet been combined.

We conclude with a consideration of how the intersection of these topics could advance membrane functionality in technologies for drug delivery and biosensing.

2.2 Biology

2.2.1 Cellular adhesion and signalling

Membrane adhesion and heterogeneity is best understood for the plasma membrane, the outermost membrane composed of lipids and proteins that encompasses all eukaryotic cells. The plasma membrane is known to be composed of groupings of specific lipids and proteins clustered into microdomains. This ordered arrangement of membrane components creates functional membrane domains specialized for cell substrate and cell-cell interactions [3, 4, 5, 6, 7, 8, 9].

A specialized microdomain that has received abundant consideration from both cell biologists and biophysicists is the raft [10, 11, 12, 13, 14, 15]. This concentration of specific lipids, largely sphingolipids and cholesterol, along with particular proteins is thought to provide a structural basis for biological function by clustering together specific components for controlled functional interactions [11, 12, 16, 17, 18, 19]. From a biophysical perspective, membrane rafts are often thought of as phase-separated domains or fluctuations in composition associated with lipid phase separation [19, 20, 21, 22, 23, 24].

These phase-separated domains play key roles in several functions of the plasma membrane. Rafts can concentrate and even order specific proteins suggesting that this microdomain can regulate protein-protein interactions [25]. The capacity of rafts to organize and thereby confer regulation to proteins has been shown in living cells where integrins, cell membrane proteins that function in cell-substrate interactions, can change conformation to adopt a higher affinity state for their ligand when in the appropriate lipid microenvironment [26, 27].

SNARES (**S**oluble **N**SF **A**ttachment Protein **RE**ceptor), proteins that function in the fusion of a vesicle with a membrane also appear to function within specialized lipid microenvironments. The association of SNARES in rafts may control their ability to function in the recognition and promotion of the fusion of a specific vesicle with its target, the plasma membrane [28, 29, 30, 31].

The concept that organization into heterogeneious specialized microdomains regulate protein function extends beyond rafts. For example specialized microdomains on the plasma membrane also play a role in immunological synapses, a structure where two immune cells interact. Immunological synapses have been shown to be sites of protein reorganization and clustering that are associated with the exchange of information between immune cells [32, 33]. This organization has important ramifications for the organism: aging is associated with changes in the lipid composition and the behavior of lipid rafts in T-cells as well as altered signaling response; it has been suggested that alterations in lipid rafts promote immune dysregulation [34].

While most examples of functional clustering of lipids and proteins into heterogeneous microdomains have been studied on the plasma membrane, the idea that ordered arrays of lipid microenvironments regulate protein function is probably true for the rest of the membranes in cells. SNARE proteins function in the fusion of vesicles with a target membrane at the plasma membrane, but also at multiple sites of membrane fusion important for organelles, including the fusion of ER-derived secretory vesicles with the cis-Golgi and other membrane fusion events in the secretory pathway. Thus it is likely that SNARES are similarly organized and regulated in microdomains in intracellular organelles. Microdomains of ordered membranes are known to provide a platform for organizing proteins into step-wise signaling cascades; organized signaling events occur throughout organelles in the cell interior. Microdomains on the intracellular membranes could well regulate the conformation affinity and function of proteins in intracellular organelles similarly to how they regulate events on the plasma membrane.

2.3 Model Systems

It is difficult, and perhaps impossible, to understand how membrane adhesion and the heterogeneous organization of membranes influence each other using living systems alone, because of the multiplicity of biological processes involved. Despite widespread observation of the importance of membrane adhesion and heterogeneities, how they are causally linked is unknown. Indeed, the origins, character, and function of heterogeneities in biological membranes independent of adhesion still have many open associated questions. Reductionist model systems provide a way around this, by al-

lowing the effects of one to a few interactions to be carefully characterized. To better understand these intricate systems, biophysical and biochemical researchers often use model lipid bilayers. Typical model membranes contain one to a few lipid species and zero to a few protein or protein-like species, depending on the purpose of the investigation.

2.3.1 Model systems for membrane adhesion

In Figure 2.1 we summarize the effects that adhesion could have on a simple bilayer membrane. Note that some effects, such as adhesion-induced tension, are expected to apply across the whole membrane, whereas other effects are localized to the adhering region or even to single proteins. Although there are exceptions, as a general rule of thumb the more global effects arise from generic physics and the more localized effects arise from molecular specificity.

The artificial giant unilamellar vesicle (GUV) has been widely used to mimic cell membranes. GUVs are typically 5-50 μm in diameter – the size of a typical eukaryotic cell. Supported lipid bilayers (SLBs) are widely used as targets for GUV adhesion. Adhesion can be mediated either by nonspecific, generic interactions or by specific protein-protein binding. It is our view that for model systems to truly yield insight into the relationship between membrane adhesion, protein heterogeneities, and lipid heterogeneities, mixed-lipid membranes near a phase transition should adhere to a target via proteins or model proteins. A substantial body of work using GUV and SLB systems with binding proteins, both model (e.g. biotin-avidin, RGD-capped lipids [35, 36], and DNA-capped lipids [37, 38]) and real (e.g. cadherin [39]), has examined the biophysics underlying the static structure and the dynamic distribution and redistribution of membrane proteins at adhesion sites [40, 41, 42, 43, 44, 45, 46, 47, 48, 49, 50, 51, 52, 53, 54, 55].

Microscopy techniques suitable for studying specific adhesion in model systems have developed in parallel with experimental models. Reflection interference contrast microscopy (RICM) has been widely used to study specifically adhering membranes [40, 41, 42, 43, 44, 45, 46, 47, 48, 49, 50, 51, 52, 53, 54, 55, 56, 57]. RICM uses the lipid membrane as one reflecting surface of an interferometer and the adhesion target substrate as the other reflecting surface. This allows RICM to measure target-membrane separations with a spatial resolution set by the wavelength of illuminating

light. RICM was originally adapted for imaging lipid membranes [56] and has been well reviewed by earlier writers [44].

Epi-fluorescence studies of specific adhesion often rely on conjugating fluorescent dye molecules to binding proteins (typically advin) as a way to visualize the location of binding proteins [40]. Total internal reflection fluorescence microcopy (TIRF) is another fluorescence-based technique suitable for measuring membrane adhesion [58]. TIRF uses the evanescent wave of a totally-reflected laser beam to excite fluorophores. Because the evanescent wave decays exponentially with distance above the reflecting surface, this provides a sensitive measure of membrane-target separation. These and other fluorescence-based techniques are reviewed in detail by Groves et al. [59].

The literature studying how adhesion processes lead to heterogeneities in the distribution of binding proteins commonly refers to the formation of protein-dense regions at the adhesion site as "phase separation". This terminology may be confusing to the reader new to the field, since this is not the lipid phase separation discussed in the section below. This field of work has primarily studied the roles of membrane mechanics, binder density, and adhesion energies, and how these interplay [40, 41, 42, 43, 44, 45, 46, 47, 48, 49, 50, 51, 52, 53, 54, 55, 60, 61, 62, 63, 64].

2.3.2 Adhesion statics

Studies using RICM and epi-fluorescence microscopy to measure model systems consisting of protein-decorated GUVs adhered to SLBs have revealed that adhesion is mediated by the formation and growth of adhesion plaques, i.e. regions where protein binders are dense (biotin-avidin 1-5% [40]) and intermembrane distances are small (for biotin-avidin the intermembrane distance is 1–5 nm, [60]and for RGD-integrin the intermembrane distance is 5–10 nm [61]). In mature adhered membranes—membranes whose adhesion zone has stopped growing—there are two primary regimes characterized by 1) complete adhesion zones composed of a single uniform adhesion plaque and 2) incomplete adhesion zones composed of adhesion plaques coexisting with regions of low binder density and large intermembrane distances (for biotin-avidin the intermembrane distance is 10-20 nm [40], [60]). The two regimes of mature membrane adhesion can be controlled by binder concentrations. For biotin-neutravidin binding Fenz et al. [40] found incomplete adhesion for initial neutravidin concentrations on the SLB less than 1% and complete adhesion for concentrations greater than 1%.

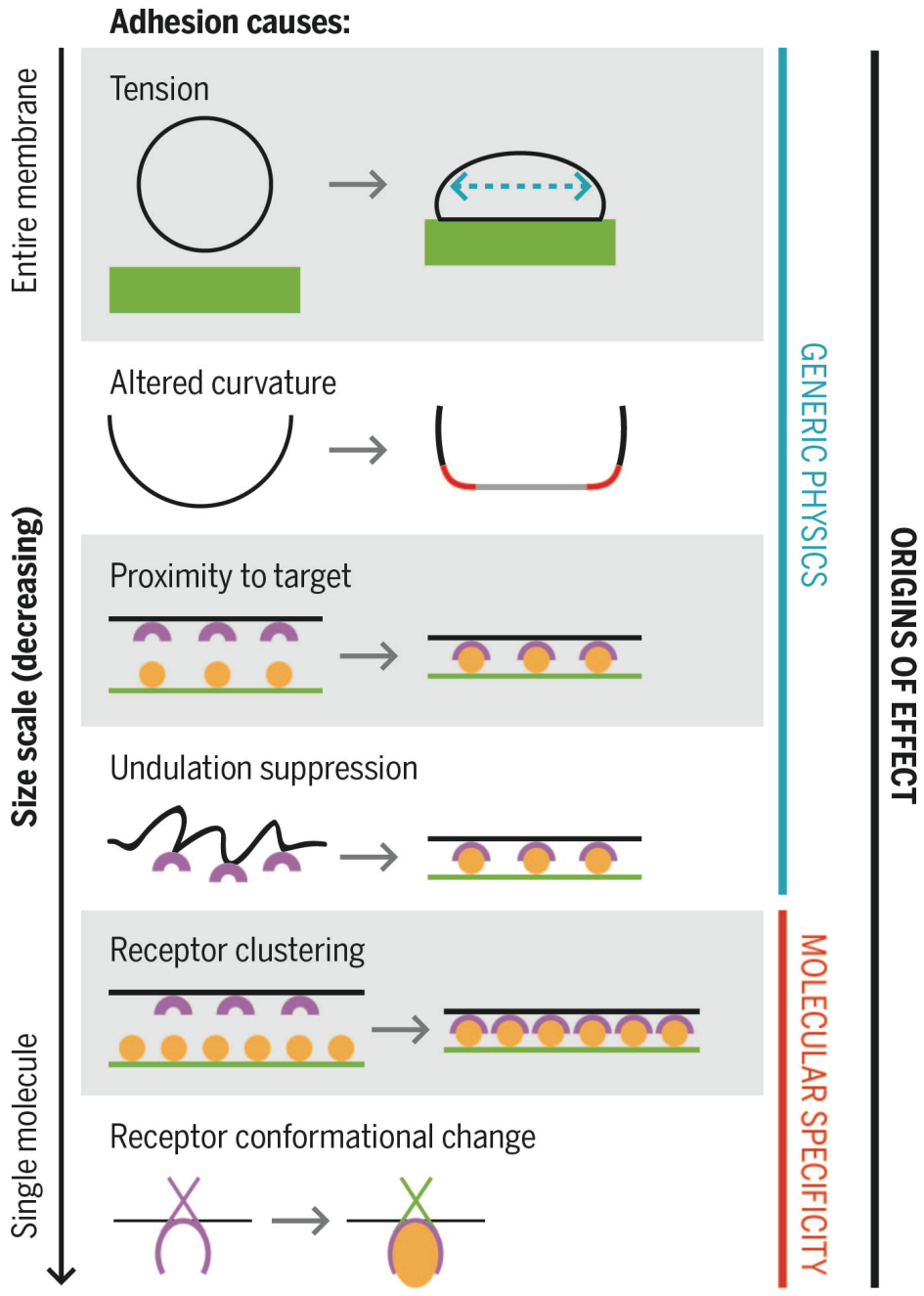

Figure 2.1: (Continued on the following page.)

Figure 2.1: **Effects of adhesion on a spherical membrane**. **(Tension)** The area of membrane adhesion will increase until binding proteins are saturated or the free energy benefit to forming one more bond is balanced by the free energy penalty for tensing the membrane by the amount necessary to form one more bond. Assuming constraint on the membrane?s internal volume, this will result in increasing the tension in the membrane. **(Altered curvature)** For the case of an initially-spherical membrane adhering to a flat, rigid target, as shown, the membrane curvature in the adhered region will be zero (grey), the membrane curvature in the non-adhered membrane may decrease or may be essentially unaltered from the initial curvature (black), and the membrane just off the adhering area will be highly curved (red). Adhesion to non-flat or non-rigid targets can also result in changes in curvature. **(Proximity to target)** Many biological membranes and model membranes contain lipids conjugated with polymers in the bilayer that prevent nonspecific adhesion (not shown). In addition, membranes are subject to thermally-driven undulations by the same principle as Brownian motion. Both these act to increase the average distance from the membrane to any adhesion target. Upon adhesion, the proximity to the target is both reduced and stabilized. **(Undulation suppression)** Thermally-driven membrane undulations will be suppressed in the adhering region, because adhesion acts to increase the free energy cost for separating the membrane from the target. **(Receptor clustering)** If the availability of targets is sufficiently high, and the free energy of binding sufficiently large, the receptors in the membrane will demix from their initially-isotropic distribution and become clustered at the adhesion site. This will result in the adhering part of the membrane being enriched in receptors, and the non-adhering part of the membrane being depleted in receptors. **(Receptor conformational change)** In biological systems, adhesion to a ligand often induces a change in the receptor that makes it more susceptible to phosphorylation or some other change on the cytoplasmic side. This is often the basis for signal transduction. It has been speculated that membrane rafts may be stabilized by changes in receptors that alter their affinity for specific lipid species or for generic characteristics of phase structure. (Adapted from [1])

Membrane adhesion causes there to be an average tension applied to the proteins binding membranes together. Therefore, the thermal energy required to break a bond between proteins bound between membranes is lower than the energy required to break a bond between proteins in free solution. For biotin-avidin in free solution, the binding energy is about -35 kT. In incompletely-adhered membranes, the energy required to break a biotin-avidin bond is only about -10 kT. A reduction in the amount of thermal energy needed break the bond of proteins binding membranes together, compared with free solution, has also been observed in the intrinsically weaker bonding pair sialyl-LewisX—E-selectin [42].

2.3.3 Adhesion dynamics

The kinetics of growth of adhesion zones give rise to adhesion dynamics. Puech et al. [46] were able to switch between two growth regimes by varying the initial tension, and thus the excess membrane area, in GUVs before adhesion. When initially-tense (tension 10^{-5}–10^{-4} N/m) membranes were adhered to an SLB via biotin-streptavidin binding, they nucleated a single adhesion plaque which proceded to a state of complete adhesion. The radial growth of the adhesion zone scaled as time$^{0.2}$ and the growth of adhesion zones stopped after about 800 s. When initially-floppy vesicles (tension 10^{-7}–10^{-6} N/m) were adhered under otherwise identical conditions, many adhesion plaques nucleated and then coalesced. In this case, radial growth of the adhesion zone scaled as time^{1} and the adhesion zones stopped growing after about 400 s. This is a striking demonstration that membrane mechanics can impact the kinetics of adhesion, in addition to the equilibrated adhered state.

The growth rates of adhesion zones have also been observed in systems where GUVs containing RGD proteins adhered to stationary integrins adsorbed onto a glass substrate [61]. This contrasts with the biotin-avidin mediated adhesion discussed above, in which avidin binders were mobile in the SLB substrate. Boulbich et al. [61] found that when the RGD contentrations in the GUVs were low (less than 0.08–0.1 mol%) the radial growth of the adhesion zone grew as time$^{1/2}$ and the adhesion region stopped growing after 1500-2000 s. However, when RGD concentrations in the GUVs were high (0.2–2 mol%) the radial growth of the adhesion zone grew as time^{1} and adhesion arrested after 30 s. The slow-growth regime was limited by RGD proteins on the GUV membrane diffusing into the adhesion front on the vesicle while the fast-

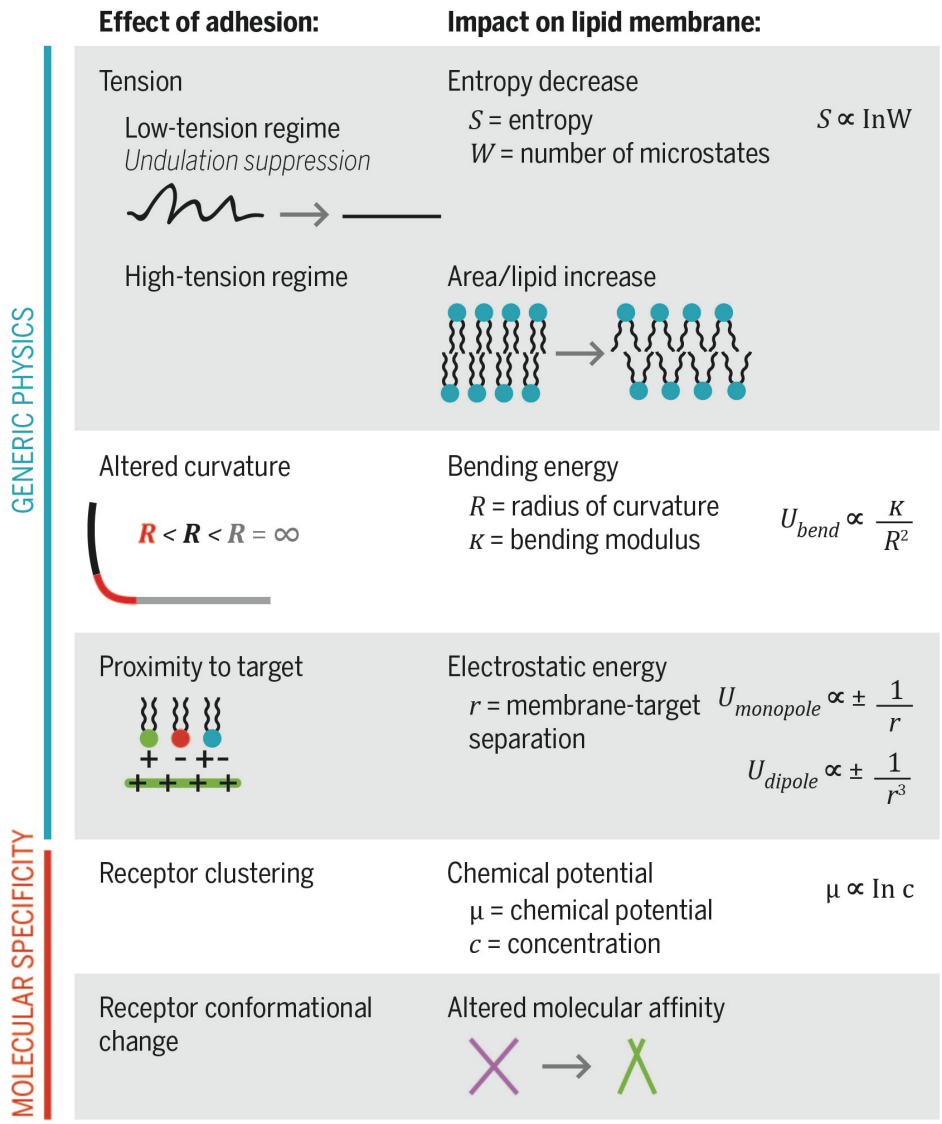

Figure 2.2: (Continued on the following page.)

growth regime was limited by the RGD-integrin binding rate. This is an example of how the chemical properties of the membrane, here in the form of the chemical potential of the RGD proteins, can impact the kinetics of adhesion.

In Figure 2.2, we summarize the changes in the physics and chemistry of a lipid bilayer membrane that could arise from the effects of adhesion described in Figure 1.

Figure 2.2: **Impacts of adhesion on membrane chemistry and physics**. **(Tension)** Work by Evan Evans and co-workers has shown that there are two regimes of membrane tension [65] a low-tension regime in which tension primarily acts to reduce thermally-driven membrane undulations, and a high-tension regime in which tension acts to increase the area per lipid. Membrane undulations increase the number of microstates available to any given macroscopic configurations, and therefore increase membrane entropy. Therefore, suppressing membrane undulations will decrease the membrane's entropy. Membrane undulations can also be suppressed directly as a result of adhesion, as indicated in Figure 1. This will also reduce the membrane's entropy in the adhered region. In the high-tension regime, increasing area/lipid is analogous to increasing volume/molecule in a gas or liquid. It increases the membrane's free energy by exposing hydrophobic lipid tails to water. **(Altered curvature)** The greatest change (per unit membrane area) in bending energy will happen in the rim membrane just off the adhering area. This rim is shown in red. Depending on the curvature of the initial, non-adhered membrane, the change in curvature from the spherical region (black) to the flat region (grey) may also result in a comparable change in bending energy. The rim region (red) will have a higher bending energy than the non-adhered, spherical membrane, and the adhered region (grey) will have a lower bending energy than the non-adhered, spherical membrane. **(Proximity to target)** Lipid headgroups are either zwitterionic or charged, as are the materials in their binding environment. This opens up the possibility of electrostatic interactions, the strength of which depends on the distance between membrane lipids and the target or other objects. For physiological conditions or work done using physiological buffers, it is also necessary to account for the screening of electrostatic interactions that arises from counter ions. The Bjerrum length gives the lengthscale at which the electrostatic interaction between two objects is comparable in magnitude to randomizing thermal energies. It depends inversely on the dielectric constant of the medium, which will be impacted by the number density and valance of salt ions. **(Receptor clustering)** The chemical potential of a species is determined by both its number density and its activity, which can be thought of as proportional to its energy level. Here we consider only the effect of concentration. Entropy maximization requires minimization of chemical potential, such that each species is isotropically distributed and at the same average number density everywhere in the system. If favourable binding energies cause receptors to concentrate in the adhering area and be depleted in the non-adhering membrane, the membrane's entropy will be reduced. Moreover, the receptor concentration will result in an increased chemical potential for the receptor species in the adhering area. (Adapted from[1])

2.3.4 Model systems for lipid phase separation

Biophysical work motivated by the desire to better understand rafts in the plasma membrane has focused on the formation of lipid sub/super-micron sized heterogeneities by lipid phase separation in artificial and biological membranes [66, 67, 68, 69, 70, 71, 72, 73, 74, 75, 76]. The liquid-ordered phase L_o is widely considered as a model phase for membrane rafts because it is rich in cholesterol and detergent insoluble lipid species. Model systems for lipid phase separation are typically ternary, containing a low-melting phospholipid, a high-melting sphingolipid (or phospholipid), and cholesterol or another sterol. The phase diagrams of such systems contain a region where L_o coexists with the fluid-disordered phase, L_d, which is widely considered as a model phase for the non-raft portion of the plasma membrane.

Synthetic model membranes are typically made with a well-defined mixture of lipids and are made at temperatures above the chain-melting temperature of the highest-melting lipid in the system. Electroformation is probably the most widely-used method for forming GUVs, because it produces a high yield of unilamellar vesicles that are tens of microns in diameter, and therefore well-sized for study with optical microscopy [77]. For visualization of phase separation using fluorescence microscopy, fluorescent dyes are incorporated into the membrane at trace amounts (typically 0.1-0.5 mol%). These dyes are preferentially excluded from or included into the lipid phases that form, according to the molecular compatibility of the dye with the lipid phase structure [78].

In other studies, researchers have investigated lipid phase separation in giant plasma membranes vesicles (GPMVs) harvested from living cells. GPMVs maintain much of the chemical complexity of living cells. A recent protocol by Sezgin et al. [66] details how to isolate, fluorescently label, and induce phase separation in GPMVs.

Upon a temperature quench, GUVs and GPMVs can undergo L_d–L_o phase separation. In their seminal work, Veatch and Keller experimentally mapped the full three-component phase diagram for DPPC/DOPC/Chol membranes [76]. This work and other work on other ternary systems [70, 79] serve as a basic library for other researchers investigating phase separation in ternary GUVs. Included in these works are the phase coordinates of the associated thermodynamic critical points where compositional fluctuations exist at the submicron scale. Suprisingly, GPMVs exist near a compositional critical point [21]. The submicron scale of composition fluctuations

in GUVs and GPMVs is the same scale as lipid rafts. This suggests biology may use critical lipid compositions as a mechanism for small scale membrane heterogeneity.

Recently, Stanich et al. studied the dynamics of phase separation in membranes that all underwent a rapid temperature quench [80]. They measured the growth of L_o domains in membranes near a miscibility boundary for membranes at both critical and noncritical compositions. They found that in critical membranes the radius of ordered-phase domains grew as time$^{0.5}$ while in noncritical membranes the radius grew as time$^{0.28}$. This is an example of controlling the kinetics of lipid phase separation by controlling the system's location on a phase diagram.

2.3.5 Membrane mechanics and phase separation

Coarse-grained approximations that treat the membrane as a continuum are often used to calculate membrane mechanics. The elastic energy cost to bend a membrane is described by the Helfrich Hamiltonian [81]. This elastic energy cost will depend on the radius of curvature R and on the bending modulus κ (Figure 2). The bending modulus is higher for ordered lipid phases than for disordered lipid phases. In addition, Brochard et al. describe the energy cost for stretching the membrane [82]. Ordered lipid phases have lower area/lipid ratios than disordererd lipid phases. Taken together, these findings suggest that altering membrane mechanics could alter the phase separation behaviour of membranes.

Recent publications have reported seemingly-contradictory effects of increasing membrane tension on the L_d–L_o demixing temperature [83, 84]. Namely, membranes that were tensed by micropipette aspiration experienced a consequent reduction in demixing temperature, but membranes that were tensed by osmotic stress experienced a consequent increase in demixing temperature. We suggest that these two sets of observations may not, in fact, contradict each other, but rather correspond to the two different regimes of membrane tension [65]. Lower tension corresponds to suppressing membrane undulations, which we expect [85] to increase the demixing temperature by decreasing the system's entropy. Higher tension increases the membrane area per lipid, which we expect disfavour ordered-phase formation and thus decrease the demixing temperature. Understanding the role of membrane tension in phase separation is relevant to biology because tension has been suggested as a possible cause of the apparent size-limitation of phase-separated domains in living

cells [86].

Other researchers have studied how altering gross (micron-scale) curvature affects the spatial segregation of pre-formed lipid phases. They formed supported bilayer membranes on corrugated solid substrates that had periodically-varying radii of curvature, and showed that L_o domains segregated to regions of lower curvature, leaving the higher-curvature regions covered with the softer L_d phase [87].

In our previous work [85], we suggested that the suppression of thermally-driven membrane undulations should favour the formation of ordered phases when the membrane is near a demixing transition. For typical GUV sizes (10 μm radius), we estimated that the shift in the free energy of demixing due to undulation suppression was of the order kT while the shift in the free energy of demixing due to gross curvature modulation was much smaller, of the order 10^{-4} kT [85]. However, the two effects become comparable when the vesicle's radius becomes about 100nm. This suggests, as Parthasarathy et al. point out, [87] that the submicron scale of lipid rafts may make rafts susceptible to curvature modulation of phase separation.

2.3.6 Model systems for lipid phase separation combined with adhesion

Other researchers have shown that the distribution of molecular species in adhering membranes can be controlled by whether binding agents preferentially partition into the L_o or L_d phases [88]. More recently, Zhao et al. have found that, near a critical point in the lipid phase diagram, adhesion produces heterogeneities in membrane components that is specific to the molecular affinity of the binder-conjugated lipids [89]. In our lab, we have found that adhesion can form dual, simultaneous heterogeneities that have protein and lipid composition distinct from each other and from the non-adhered portion of the membrane [2]. We suggest that this likely results from an interplay between physical interactions associated with adhesion mediated by proteins, which will locally suppress membrane undulations, reduce curvature, and modify tension, and the molecular structure of the protein-conjugated lipids, which will have an affinity to one or more components of the lipid membrane and a disaffinity to the ordered phase structure.

In addition to the experiments summarized in the previous paragraph, there are theoretical models examining the effects of adhesion on lipid phase separation in

membranes [90, 91]. One reason that theory is powerful is that it allows the behavior of a complex system to be described as a function of only the salient parameters. Unfortunately, in the case of the interaction between adhesion and phase separation, it is not known what controlling parameters are relevant in specific cases. What parameters matter is likely to depend sensitively on details such as the molecular structure of lipid species in the membrane, the system's location on its phase diagram, the molecular structure and mechanical compliance of adhesion-mediating binding proteins, the topography and compliance of the target for adhesion, and the mobility of binding proteins in the membrane and the target.

Figure 2.3 summarizes different ways that adhesion could impact demixing in a mixed-lipid membrane. These ideas are grounded in fundamental principles of lipid chemistry and physics and, to some degree, by empirical studies. However, we emphasize that these ideas are speculative and the degree to which the described effects will impact specific systems very much remains to be determined.

2.4 Technology

2.4.1 Encapsulation and controlled release of therapeutic agents

In the clinic and home, lipids and lipid-like amphiphiles are widely used in technologies for controlled encapsulation and release [92, 93, 94, 95, 96, 97, 98]. Liposomes can significantly improve circulation times and can overcome many of the biophysical barriers to drug uptake and effectiveness. In liposome-based systems, delivery is often triggered when the membrane phase separates laterally, into co-existing fluid and solid phases [99]. How phase transitions promote release is not generally understood.

Phases vary in their lipid packing density, and so may have varying permeability to drugs, or domain boundaries may have more defects and therefore be more permeable than continuous regions of any phase [99, 100, 101, 102, 103]. It has also been proposed that physiologically-present proteins act at domain boundaries to disrupt the liposome and increase release [104]. These mechanisms would tend to favour slow, diffusive release, while the disruption in the membrane inherent to the phase transition itself could allow a transitory "burst" of release.

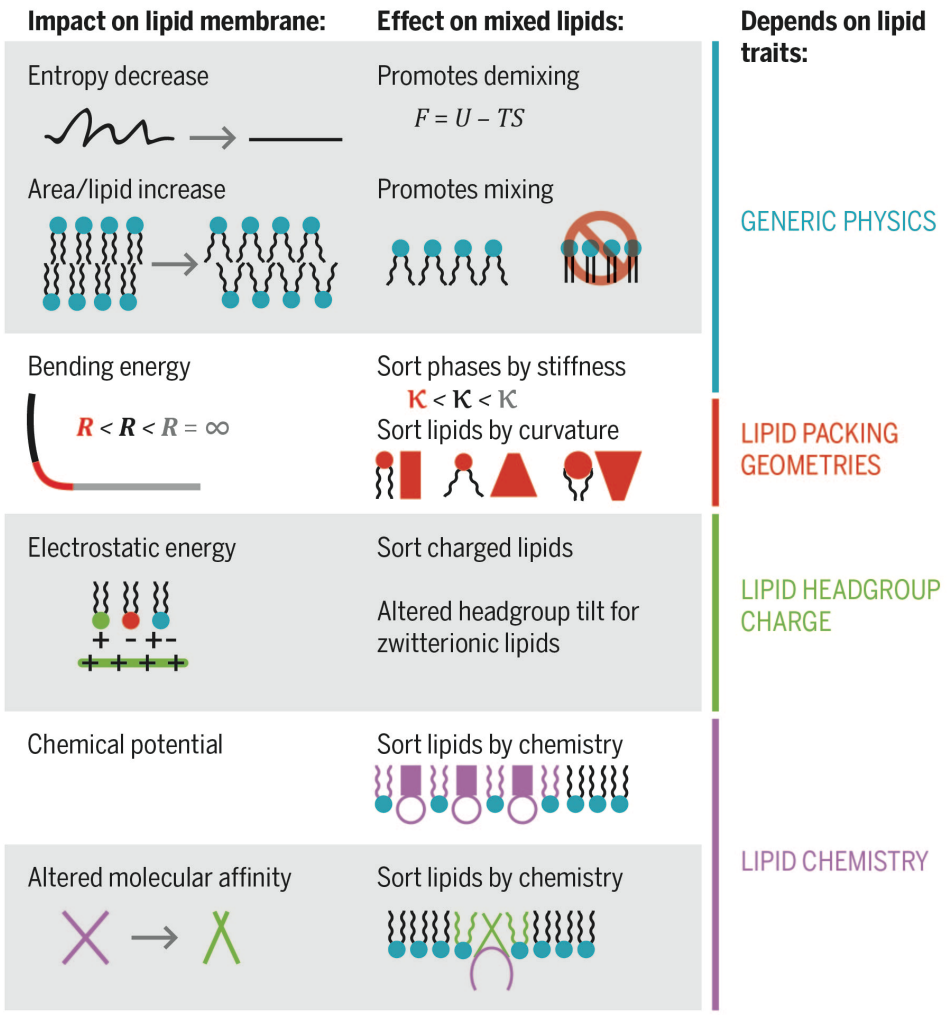

Figure 2.3: (Continued on the following page.)

Thermally-triggered phase transitions in the membranes of vesicles delivering drugs to hyperthermic cancer sites [105] have gone to clinical trials [106]. Typically, the targeted site must be at 43 °C, whereas normal human body temperature is 37 °C. Since body temperatures above 40 °C can be life-threatening, induced hyperthermia at the target site must be spatially minimized and carefully controlled. This has been one of the significant obstacles to overcome for this type of therapy, and has limited its application to sites that can withstand elevated temperature, and where such elevation in temperature can be restricted to the target area only.

Much work exists to target delivery from membrane-based encapsulation sys-

Figure 2.3: **Potential impact of adhesion on lipid demixing**. **(Entropy decrease)** Systems demix when this will minimize their free energy, $F = U - TS$. Thus, for equilibrium physics, the conditions determining whether a membrane will be mixed are demixed are set by a competition between energetic and entropic terms. We have previously argued that suppressing undulations should act to favour demixing by reducing the entropic cost of demixing to form a stiffer lipid phase. **(Increased area/lipid)** By Le Chatelier's principle, which states that an equilibrated system will respond to an externally-imposed change in such a way as to oppose the change and achieve a new equilibrium, we expect area/lipid dilation to promote mixing because the area per lipid is greatest for the fluid-disordered L_d phase, and lower for L_o and other ordered lipid phases. **(Altered curvature)** Work by others has suggested that changes in curvature alone could cause the membrane to phase separate and localize stiffer phases in regions of low curvature, and softer phases in regions of high curvature. **(Proximity to target)** Minimization of electrostatic energy will sort species of the opposite charge sign to be near the target, and species of the same charge sign to be away from the target. Dipole interactions could alter the tilt of lipid headgroups. Since different lipid phase structures have different headgroup tilts, in principle this could favour demixing. **(Receptor clustering)** If the receptors have a specific affinity for a particular lipid species, that species could be concentrated in the adhesion region of the membrane. This has recently been shown by Sarah Veatch and co-workers. **(Receptor conformational change)** If a receptor undergoes a change upon adhesion that alters its affinity for a particular lipid species, that could promote demixing on a very local, molecular lengthscale. We note that this effect does not depend on adhesion to a large or solid target, but could happen even for receptor binding to a small, soluble ligand. Therefore, while it may be challenging to achieve in a model or technological system, this likely under-reflects its biological importance. (Adapted from [1]).

tems by incorporating specifically-binding proteins into the membrane. Specifically-binding proteins bind to a particular ligand or target profile. Tumors may be targeted by EGF [107, 108], transferrin and its receptor [109, 110, 111], the RGD sequence [112], or the metastasis-asociated Eph A2-EphrinA1 pair [113]. Other binders include T cell receptors and their cognate ligands [113], collagen-binding block copolymers [114] and peptides [115], artificial extracellular matrix proteins [116], cadherins [39], and lipids capped with RGD [35, 36] or DNA [37, 38]. To date, systems of specifically-adhering membranes for drug delivery have not examined the formation of heterogeneities in the delivering membrane. However, since membrane adhesion is associated with the formation of heterogeneities in protein and lipid composition

and phase, we suggest that there is likely technological potential for membranes that respond to adhesion by forming heterogeneities without requiring harmful elevations in temperature.

2.4.2 Biosensing

By containing many signalling molecules, lipid vesicles have the ability to transduce a signal from one or a few binding events into a many-molecule signal. This approach is widely used in biosensors [117] in which liposome binding to a specific region on a strip is controlled by analyte concentration. Subsequent processing, typically involving washing-away or lysis of liposomes, results in a readable signal. Liposome-based sensors have been used to detect a variety of harmful agents and disease markers [118, 119, 120, 121, 122, 123, 124, 125, 126, 127, 128, 129, 130, 131, 132, 133, 134, 135, 136, 137, 138, 139, 140, 141, 142, 143, 144] and often have good sensitivity and easy readout. Reducing the number of steps involved in a biosensor assay improves that assay's efficiency and ease of use. Thus, it is desirable to have liposomes that respond to binding per se by some detectable signal. One avenue toward such responsive liposomes may come from phase separation of bilayer membranes, as in the previous section. Therefore, controlling the characteristics of adhesion-induced phase separation presents a possible way to control signal amplification in biosensors.

Figure 2.4 summarizes some speculative avenues by which the release of encapsulated contents might be tuned by changing either the perimeter/area ratio of ordered phase and/or the timescale of lipid phase separation, using some of the biophysical ideas discussed previously and shown in Figures 1-3.

Figure 2.4 focuses on cases in which the encapsulating membrane stays intact, but poration or lysis of the membrane could also be a good strategy for content release. Lateral clustering of negative-curvature or fusogenic lipids may favour membrane poration, lysis, and fusion [145, 146, 147, 148, 149, 150, 151].

2.5 Conclusions

The interplay between protein-mediated adhesion and lipid phase separation is greatly under-studied and ripe for growth. Extant streams of work that separately examine membrane physics, protein-mediated adhesion, and lipid phase behavior have laid

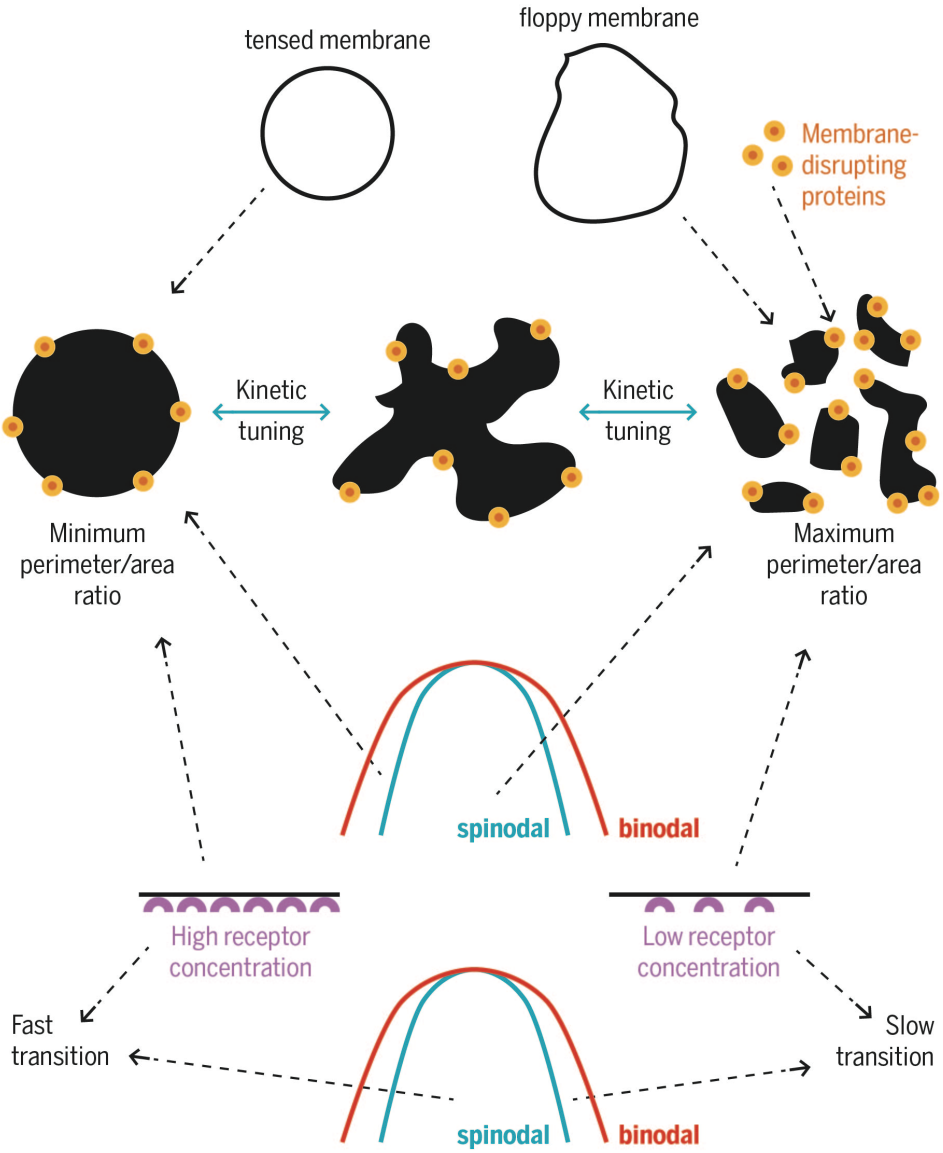

Figure 2.4: **Potential avenues for tuning the release of encapsulated contents by tuning the perimeter/area ratio of ordered domains and/or the speed of the phase transition**(These suggestions are based on the impact of mechanical and compositional parameters on membrane adhesion and lipid phase separation, as discussed in the text. In addition, we note that the speed of a phase transition can also be changed if the composition of the membrane can be adjusted such that a first-order transition is replaced with a second-order transition, or vice versa. A second-order transition will be slower than a first-order transition.) (Adapted from[1]).

a firm foundation for a new research area that synthesizes these streams. A better understanding of how specific adhesion and lipid phase separation interact has the potential to advance both biology and technology. Both the generic physics of a flexible membrane and the specific chemistry and molecular structure of the protein and lipid species involved are likely to play important roles, as is the mechanics and molecular specificity of the target for adhesion. This rich landscape of parameters provides a biophysical and biochemical rationale for the different types of membrane heterogeneities found at adhesion sites of biological membranes. This review has focused primarily on adhesion to external structures, but the scaffolding cytoskeleton is an internal structure that also has the potential to impact membrane structure. Adhesion to a soluble ligand could also produce some of the same biophysical interactions discussed here.

Chapter Three: Specific adhesion of membranes simultaneously supports dual heterogeneities in lipids and proteins

Membrane adhesion is a vital component of many biological processes. Heterogeneities in lipid and protein composition are often associated with the adhesion site. These heterogeneities are thought to play functional roles in facilitating signalling. Here we experimentally examine this phenomenon using model membranes made of a mixture of lipids that is near a phase boundary at room temperature. Non-adherent model membranes are in a well-mixed, disordered-fluid lipid phase indicated by homogeneous distribution of a fluorescent dye that is a marker for the fluid-disordered (L_d) phase. We specifically adhere membranes to a flat substrate bilayer using biotin-avidin binding. Adhesion produces two types of coexisting heterogeneities: an ordered lipid phase that excludes binding proteins and the fluorescent membrane dye, and a disordered lipid phase that is enriched in both binding proteins and membrane dye compared with the non-adhered portion of the same membrane. Thus, a single type of adhesion interaction (biotin-avidin binding), in an initially-homogeneous system, simultaneously stabilizes both ordered-phase and disordered-phase heterogeneities that are compositionally distinct from the non-adhered portion of the vesicle. These heterogeneities are long-lived and unchanged upon increased temperature.

3.1 Introduction

Adhesion of a biological membrane to another membrane or an extracellular matrix substrate is a widespread phenomenon in biology. Membrane adhesion is requisite for many vital biological processes, including exocytosis, intracellular trafficking, and sexual reproduction. Heterogeneities in the lipid and protein composition of the membrane are often associated with adhesion sites; these heterogeneities are frequently known as "rafts" and are thought to facilitate signalling by clustering together proteins with an affinity for the liquid-ordered lipid phase that characterizes the raft [10, 12, 13, 14, 15, 152]. To elucidate the biophysical principles undergirding raft

formation, experimental physical scientists have often used simplified experimental model systems in the form of giant unilamellar vesicles (GUVs) that are typically made of a high-melting lipid, a low-melting lipid, and a sterol. Such biophysical studies have largely focused on lipid phase separation at thermodynamic equilibrium, [75, 76, 79, 83, 84, 85, 153] and on the effects of biologically-relevant perturbations such as tension [83, 84] and curvature [87] and undulations [85]. We have previously shown that non-specific membrane adhesion can promote the formation of an ordered lipid phase [85].

Traditionally, specific adhesion of membranes via protein-like binders [40, 57, 60, 61, 62] has been studied separately from lipid phase separation. Specific adhesion can produce heterogeneities in binding-protein distribution via equilibrium and kinetic mechanisms. It has recently been shown that, for ternary-mixture GUVs near a critical point, adhesion can stabilize compositional heterogeneities that result from the molecular affinity of the biotin-conjugated lipids, used to control binding, for the fluorescent dye that marks the disordered lipid phase [90]. However, we are far from a comprehensive understanding of the interactions of adhesion with membrane heterogeneities. This is complicated even further by cases such as the immunological synapse, in which more than one type of compositional heterogeneity is simultaneously stabilized by adhesion [154, 155, 156, 157, 158]. Understanding and controlling the interactions of adhesion and biomembrane heterogeneities will advance our understanding of fundamental biological processes and could lead to new therapeutic pathways that rectify abnormalities in adhesion-related signalling. It also will advance possibilities for making "smart," responsive membrane-based containers for technological use.

Here we show that membrane adhesion that is mediated by only one binding species can simultaneously support two different types of heterogeneity - an internal ordered-phase lipid domain surrounded by a peripheral disordered-phase lipid domain. Binding proteins are localized to the disordered-phase region of the adhesion site, which is also enriched in the disordered-phase dye compared with the non-adhered, disordered-phase portion of the membrane. The rough annular patterns that adhesion produces are stable over the timescale of hours up to a day. Thus, we show that a single type of adhesive interaction can sort membrane components into two types of long-lived, heterogeneous structures. Moreover, we show that some features of these heterogeneities could be out of equilibrium. This is important, because there

are more possibilities for tuning the properties of membrane heterogeneities if out-of-equilibrium states are accessible.

3.2 Materials

The lipids used in this study were purchased from Avanti Polar Lipids: 1,2-dioleoyl-sn-glycero-3-phosphocholine (DOPC); 1,2-dipalmitoyl-sn-glycero-3-phosphocholine (DPPC); 1,2-diphytanoyl-sn-glycero-3-phosphocholine (DiPhyPC); cholesterol (Chol); 1,2-dioleoyl-sn-glycero-3-phosphoethanolamine-N-(cap biotinyl) (sodium salt) (biotin-DOPE); and 1,2-dioleoyl-sn-glycero-3-phosphoethanolamine-N-[methoxy(polyethylene glycol)-2000] (ammonium salt) (PEG-DOPE). PEG-2000 has a radius of 1.2-1.6 nm measured by small-angle neutron scattering [159]. Binding proteins and dyes were purchased from Invitrogen: BODIPY® Fluorescent membrane dye (Bodipy); Avidin, NeutrAvidin Biotin-binding Protein (neutravidin); Avidin, NeutrAvidin®, Oregon Green® 488 conjugate (neutravidin-488); and DiI fluorescent membrane dye (1,1'-Dioctadecyl-3,3,3',3'-Tetramethylindocarbocyanine Perchlorate ('DiI'; DiIC18(3))) (DiI). Ultrapure 18.2 MΩcm water (DI Water) was obtained with the MilliQ Millipore system. Other reagents were purchased from Fisher Scientific: chloroform, sucrose, glucose, and DPBS Buffer 1x w/o Calcium Chloride and w/o Magnesium Chloride (PBS). All lipids purchased were already dissolved in chloroform except Chol which was purchased as powder and subsequently dissolved in chloroform. All dyes and proteins were purchased as powder; the dyes were later dissolved in chloroform and the proteins later dissolved in PBS. The lipid and dye solutions were stored in screw-cap vials at -20 °C and the protein solutions were stored at either -20 °C or, for immediate use, at 4 °C.

3.3 Methods

3.3.1 Giant Vesicle Formation

Giant unilamellar vesicles (GUVs) were electroformed [160] as follows. Lipids and dyes were mixed at desired proportions, using a Hamilton syringe, to produce a stock solution with net concentration 10-15 mg/mL. 5 μL of stock solution was deposited to form a thin film on the conductive side of clean indium-tin-oxide (ITO) -coated

glass slides (Sigma Aldrich #703192 8-12 Ω/sq). To achieve a thin film, a 5 μL drop was deposited at one side of the ITO slide and then the syringe needle was used to quickly sweep the drop across the entire slide. Coated slides were shielded from light and held under vacuum with desiccant at approximately 0.1 MPa below atmospheric pressure for 1 hr or more to remove any residual chloroform from the film. Once the vacuum was released, the lipid-coated ITO slides were assembled into a parallel-plate capacitor consisting of two ITO slides facing each other, spaced by a gasket with a narrow opening at the top. Small strips of copper tape were sandwiched between the gasket and the ITO slides on either side to act as electrical leads and the chamber was held together by binder clips. After assembly, the chamber was filled with the desired swelling solution and the gap in the gasket was covered with modelling clay (Sculpey^{TM} Oven Bake Clay). During the coating, vacuuming, and assembling processes, the lipid film contacted room air at standard pressure for approximately 1 minute maximum total time. This was done to avoid oxidation of the lipids. The assembled chamber was put into an oven at 60 °C, which is well above the chain-melting temperature of the lipid species used. A function generator was then connected across the two copper leads and an AC voltage applied in three stages. We measure voltage using its root-mean-squared (rms) value. First, the voltage function was set to a 10 Hz sine wave at 0.05 V and was increased in increments of 0.05 V in 3 min intervals until reaching 0.50 V; second, the 10 Hz, 0.50 V, sine wave setting was held for 2 hrs; third, the function was changed to a 5 Hz square wave and set to 1.20 V and held for 30 min. After completing the electroformation process, the function generator and the oven were turned off and the GUVs were allowed to cool to room temperature in situ for about 1 hr. The cooled GUVs were gently removed from the chamber using an 18-gauge syringe needle, transferred to an Eppendorf tube, and diluted with 0.75-1.00 mL of room-temperature swelling solution.

3.3.2 Small Vesicle Formation

Small vesicles (SVs) were formed by extrusion [9] as follows. Lipids and dyes were mixed in a test tube at desired proportions, using a Hamilton syringe, to a net concentration of ∼10-25 mg/mL. The solution was dried by swirling in the bottom of the tube under a light stream of flowing nitrogen. This left a film of dry lipid on the walls of the test tube. The lipid-coated tube was shielded from light and held

under vacuum with desiccant at approximately 0.1 MPa below atmospheric pressure for 1 hr or more to remove any residual chloroform from the film. 500 μL of DI water was added to the test tube, which was then vortexed until all the visible lipid was suspended in the water. The lipid suspension was then extruded in two steps using an Avanti®Mini-Extruder #610000: first, 250 μL of the solution was filtered 10 times through a 0.4 μm-pore membrane (Whatman Nucleopore 19mm #800282); second, the same solution was filtered 10 times through a 0.03 μm-pore membrane (Whatman Nucleopore 19mm #800307). The SV solution was diluted 2x with PBS and was used to form supported lipid bilayers (as described below) within 12 hours.

3.3.3 Sample Preparation

To prepare substrates for supported lipid bilayers (SLBs), we cleaned Menzel-Glaser 24x32 mm #1 cover glasses using Piranha etching, [9] using 3:1 98 % sulfuric acid: 30 % hydrogen peroxide. This made the glass surfaces very hydrophilic. Cleaned cover glasses were stored in a container filled with DI water until they were used for an experiment; cover glasses were used no more than two days after Piranha etching. For all experiments, two sample slides were prepared in parallel. One sample served as the control, in which GUVs sedimented but did not specifically adhere to the SLB. For this sample, we made an SLB as described below, but did not functionalize the SLB with neutravidin. The other sample was the test sample in which GUVs specifically adhered to the SLB via biotin-avidin binding. This SLB was prepared as described below and then functionalized with neutravidin.

We dried cover glasses using a stream of nitrogen gas, placed a rubber gasket in the centre of each glass, and sealed the gasket's edges with vacuum grease. To make SLBs, 200 μL of the SV+PBS buffer mixture was added to the centre of each gasket and allowed to sit for 30 minutes before the excess SVs were rinsed from the glass. We rinsed the SVs by adding another 200 μL of PBS buffer inside the gasket, pipetting back up, and discarding. This was repeated 15 times. Then, 50 μL of neutravidin at (75 μg/mL) was added to the designated test SLB and allowed to sit for 45 minutes. The test SLB was then rinsed, as before, and 50 μL of the prepared GUV suspension was added. The sample was then capped with a 22x22 cover glass and allowed to sit for at least 10 minutes to allow time for the GUVs to adhere. The control slide was prepared similarly, except that it was not functionalized with neutravidin.

To control the pre-adhesion tension in the GUV membranes, we tuned the sucrose solution to be iso-osmolar with the PBS.

3.3.4 Microscopy temperature control and data analysis

Membranes were imaged by epifluorescent microscopy on an Olympus IX71 inverted microscope at 100X magnification with an Olympus TIRF UIS2 UAPON objective and by confocal microscopy on an Olympus IX81 inverted microscope at 100X magnification with an Olympus UPlanFl N objective. Temperatures were controlled using a Physitemp TS-4 SPD Controller. When samples were heated, the temperature reading was calibrated to a measured temperature calibration curve which we constructed by inserting a thermocouple into one of our sample chambers and measuring the sample temperature as a function of the controller?s temperature reading. Data analysis was done in ImageJ and Matlab.

3.4 Results

3.4.1 Adhesion induces the formation of an ordered phase

We chose a 29:29:42 DPPC:DOPC:Cholesterol mixture for this study because previous work has reported that, at room temperature, GUVs of this composition are in a well-mixed, liquid-disordered (L_d) lipid phase, close to a phase boundary defining a region where (L_d) and liquid-ordered (L_o) phases coexist [76]. In three separate experiments, GUVs that included 1 mol% biotin-DOPE, 1 mol% PEG-DOPE, and 0.2 mol% DiI were electroformed and the resulting yield was split, so that some were added to neutravidin-functionalized SLBs and some to non-functionalized SLBs. The vesicles used to form the SLBs contained 98 mol% DOPC, 1 mol% biotin-DOPE, and 1 mol% PEG-DOPE. DOPC's chain-melting transition temperature is about -20 C, so the supported bilayers remained fluid throughout our studies. We verified fluidity by checking that SLBs containing Bodipy recovered after photobleaching; bilayers also appeared continuous. GUVs that were added to neutravidin-functionalized SLBs adhered specifically to the substrate via biotin-avidin binding. GUVs that were added to the non-functionalized SLBs sedimented because of the density difference between internal sucrose solution and external PBS buffer, but did not specifically adhere.

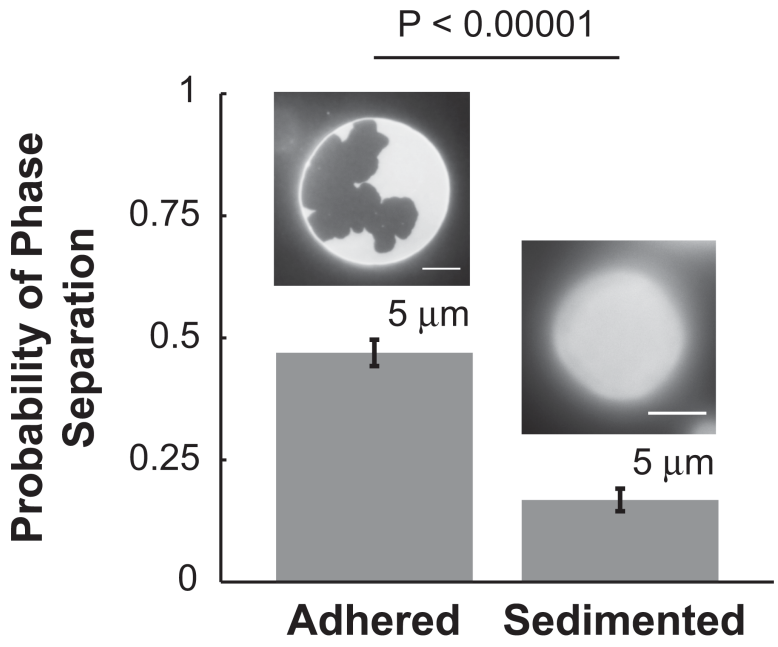

Figure 3.1: Specific adhesion promotes the formation of an ordered lipid phase in initially-homogeneous vesicles. Here we show the fractions of membranes that contained an ordered-phase domain for 370 adhered and 262 sedimented vesicles. The error bars are the standard error of the mean by approximating the binomial distributions as Gaussian. Data from three independent experiments are used. Each experiment studied adhering and compositionally-identical sedimented vesicles in parallel. (Adapted from [2]).

The fluorescent membrane dye DiI is excluded from ordered-phase domains as an impurity, so that phase coexistence between the Ld phase and an ordered phase appears as bright and dark patches respectively on vesicles. Representative images of a phase-separated and a homogeneous vesicle are shown as insets in Figure 3.1.

Of 341 specifically-adhered vesicles, 160 (47%) were phase separated and the ordered domains were almost always localized to the adhesion zone. That the ordered phase was localized to the adhesion zone is consistent with a recent theoretical prediction for two-component adhering membranes [91]. Of 262 sedimented vesicles, 44 (17%) had at least one ordered-phase domain (not necessarily localized to the bottom). These data are summarized in Figure 3.1.

To check the significance of these results, we used a binomial probability distri-

bution function

$$P(x = k) = \frac{n!}{k!(n-k)!} p^k (1-p)^{n-k} \tag{3.1}$$

to describe the likelihood that exactly k membranes phase separate out of n trials, with a probability of phase separation $p = 0.17$. This probability is taken from the sedimented vesicles' distribution. Using the cumulative distribution function of the binomial distribution, we estimate the probability of more than $k = 159$ vesicles phase separating after $n = 341$ trials as

$$P(x > k) = 1 - \sum_{i=1}^{n} \frac{n!}{k!(n-k)!} p^k (1-p)^{n-k} < 0.00001 \tag{3.2}$$

We conclude that specific adhesion significantly increases the probability that L_d lipid membranes will phase separate to form an ordered phase. Since the specifically-adhering and sedimented vesicles are otherwise identical in composition and preparation history, we infer that adhesion *per se* is the cause of the increased likelihood of forming an ordered phase.

We have previously found that non-specific adhesion—in which membranes contact each other directly, without the mediation of binding proteins—can promote the formation of ordered phases in mixed-lipid membranes [85]. In our earlier work, we suggested that this could result from adhesion suppressing thermally-driven undulations in the membrane. Undulations increase the system's entropy. Forming a stiffer, ordered phase out of the disordered fluid phases L_d or L_α will reduce the amplitude of undulations and is therefore entropically disfavoured. Adhesion pays part of this entropic cost by pre-reducing the amplitude of undulations. Other researchers have examined the role of membrane curvature in the segregation of pre-existing phases [54, 87, 161]. They found that stiffer, ordered-phase domains segregate to regions of lower curvature. This minimizes the net bending energy of the system. We have previously estimated that, for spherical membranes of the $\sim$10 μm radius typifying our GUVs, the effect of undulation suppression will be stronger than that of changes in gross curvature caused by adhesion [85]. However, in an analysis that does not consider the role of undulations, it has been suggested that adhesion-caused change in gross curvature could lead to the formation of an ordered domain upon adhesion, since the curvature is zero in the adhering region [90] if the substrate is flat. Both undulation-based and gross curvature-based interpretations assume that the formation of ordered-phase domains reduces the system's free energy. Therefore, these two

interpretations are compatible with but do not necessarily require equilibrium phase separation.

In the following Results subsections, we examine different aspects of adhered, phase-separated membranes to evaluate the degree to which they may be equilibrated and the degree to which they may not be equilibrated.

3.4.2 The ordered-phase domains are robust to increases in temperature to above the DPPC transition temperature

Lipid phase separation can result from a quench in temperature that takes a mixture of lipids across a phase boundary. A straightforward equilibrium interpretation of our results would imply that adhesion raised the temperature of the phase boundary, but not above the transition temperature of the highest-melting component of our system. We investigated the temperature response of the ordered phases formed in adhered membranes. The temperature was raised in increments of 2 °C with 5-minute intervals between to allow the sample to thermally equilibrate. We found that even when the temperature of the sample was as high as 55 °C, the ordered phase domains showed no changes in size or shape. This result is surprising because our system's highest-melting component, the lipid DPPC, has a chain-melting transition temperature of only 41 °C.

We conclude that either these membranes are far from equilibrium, or that adhesion drastically modifies the free energy landscape of the membrane. In our previous work we estimated that suppressing undulations could change the free energy of demixing by about 3kT [85]. This is inadequate to explain a shift in transition temperature of more than 14 °C. However when membranes are bound via biotin-neutravidin, there is a debinding free energy cost of about 10 kT per biotin-neutravidin bond [40]. We therefore infer that the ordered-phase domains we see in adhering regions may or may not be in thermodynamic equilibrium.

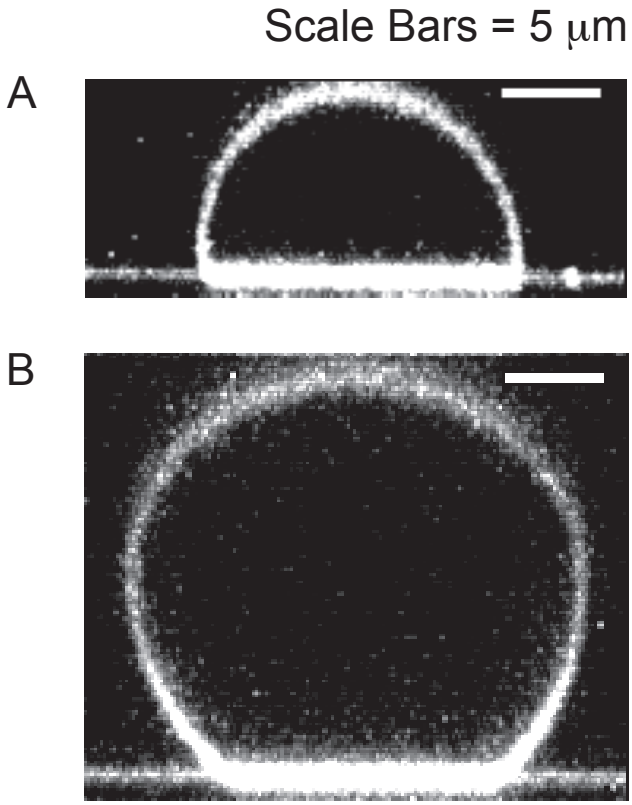

Figure 3.2: **Adhered vesicles are ellipsoids but phase-separated-vesicle geometry differs from non-phase-separated vesicle geometry.** A) A vertical slice through an adhering, phase-separated vesicle. B) A vertical slice through an adhering, non-phase-separated vesicle. (Adapted from [2]).

3.4.3 The geometry of adhering membranes suggests adhered vesicles are in mechanical equilibrium

Adhesion also modifies the shape of GUVs from their initial sphericity. We used confocal microscopy to measure the 3-dimensional shapes of adhered GUVs (Figure 3.2A and 3.2B).

Since our GUVs look spherical before adhesion, we compare the measured volume of adhered GUVs with the volume that a sphere with the same surface area would have. Strikingly, we found that adhered vesicles fall into two distinct groups. Not-phase-separated GUVs had volumes 0.975 ± 0.005 that of an equivalent-area sphere, and phase-separated GUVs had volumes 0.838 ± 0.004 that of an equivalent-area sphere (Figure 3.3D; 3.3A zooms in on the portion of this plot representing smaller

vesicles). From this, we infer that GUVs that phase separated upon adhesion lost more of their internal volume than did GUVs that did not phase separate.

We also measure the proportion of the GUV membrane that was adhered to the substrate by taking the ratio of adhering and non-adhering area for each GUV. Vesicles also fall into two distinct groups for this measurement. Phase-separated membranes have an (adhered area)/(non-adhered) ratio of 0.39 ± 0.01, whereas not-phase-separated membranes have an (adhered area)/(non-adhered) ratio of 0.13 ± 0.02 (Figure 3.3B; 3.3D zooms in on the portion of this plot representing smaller vesicles). A greater fraction of the membrane has spread onto the flat substrate for GUVs that phase separated upon adhesion than for GUVs that did not phase separate.

Mechanical equilibrium for the adhesion of spherical membranes implies that the adhered area will grow until the reduction of free energy by making one more biotin-neutravidin bond is equal in magnitude to the gain in elastic energy this bond will cause by tensing the membrane. Vesicles losing internal volume, which we find associated with phase separation, is equivalent to vesicles gaining excess membrane area. Taken together, the two sets of observations in Figures 3.3, **??** are consistent with our vesicles being in mechanical equilibrium.

3.4.4 A single thermodynamic coordinate governing whether phase separation occurs is insufficient to account for the distribution of ordered-phase domain sizes

Following the lead of other researchers, we take the miscibility transition temperature to be the temperature at which half the GUV membranes (which will have some variability in their lipid composition) phase separate; for our GUVs, the transition temperature is $\sim$20 °C in the absence of adhesion [76, 79]. When our membranes adhere, half of them are phase separated at room temperature, which is nearly 24 °C (Figure 3.1).

With only half the adhering vesicles phase separating, a single-coordinate equilibrium view implies that only half the GUVs have an adhesion-shifted demixing transition temperature greater than room temperature. This implies that the high-melting

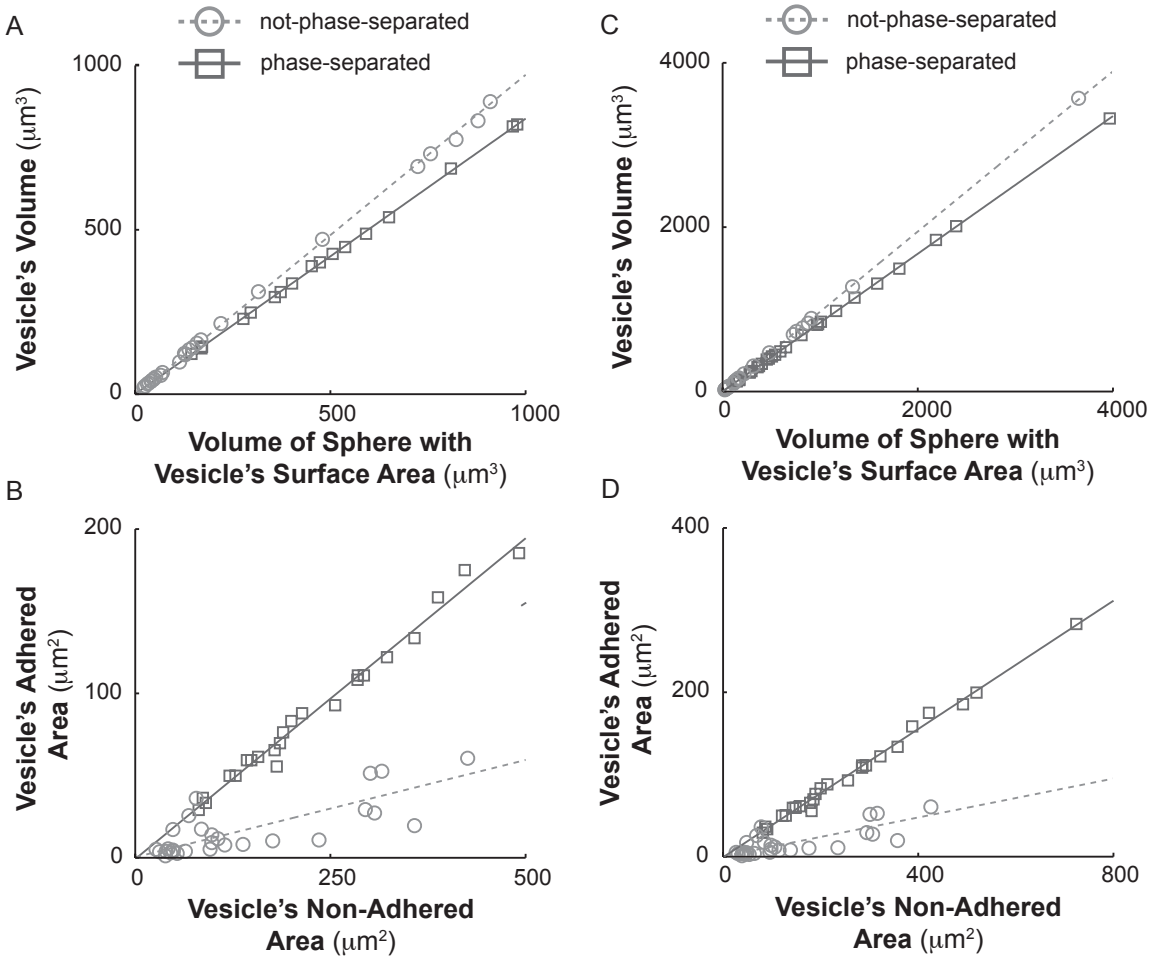

Figure 3.3: **Adhered vesicles' geometries have two distinct states:** one for phase-separated vesicles and another for not-phase-separated vesicles. A) and C) The ratio of adhered vesicles' volume to the volume of spheres whose surface areas are the same as the vesicles' surface areas. Dark grey squares are phase-separated vesicles with a solid-line fit whose slope is 0.838±0.004 and $R^2 > 0.99$. Light grey circles are not-phase-separated vesicles with a dashed-line fit whose slope is 0.975 ± 0.005 and $R^2 > 0.99$. B) and D) The ratio of adhered vesicles' adhered surface area to the non-adhered surface area. Dark grey squares are phase-separated vesicles with a solid line fit whose slope is 0.39±0.01 and $R^2 > 0.99$. Light grey circles are non-phase-separated vesicles with a dashed-line fit whose slope is 0.13±0.02 and $R^2 > 0.87$. The reported uncertainties are the 95% confidence intervals. (Adapted from [2]).

lipid distribution peaks for the lowest composition for which phase coexistence is observed, and that in the coexistence region (grey shading) vesicles with larger high-melting lipid content should occur with decreasing frequency (Figure 3.4A).

According to the "lever rule" [162], the amount of ordered-phase area should grow with the fraction of high-melting lipids. However, this is not what we observe. Instead, we find that the frequency distribution of ordered-phase area fraction is roughly symmetric about an area fraction of 0.22 ± 0.03 (Figure 3.4B). This suggests that whatever parameters cause an adhered membrane to nucleate an ordered-phase domain are not the same as the parameters that determine the final amount of ordered phase formed.

We infer that either another thermodynamic coordinate is necessary to explain an equilibrium distribution like what we measure, or lipid-driven phase separation is being competed with by non-equilibrium interactions that originate from the protein binders

3.4.5 The shapes of ordered-phase domains in adhering membranes are inconsistent with equilibrium separation of fluid lipid phases

Equilibrium thermodynamics can also inform expectations about the shape of phase-separated domains. It is well-established from previous work that fluid-phase domains, whether their phase is liquid-ordered (L_o) or liquid-disordered (L_d), will have circular shapes at equilibrium [75, 153]. A circular perimeter minimizes the total boundary between phases and thereby minimizes the total line tension and the energy of the system. However, the ordered-phase domains in adhesion zones are not circular.

We quantified the circularity of ordrered-phase domains using the measure

$$circularity = 4\pi \frac{area}{circumference} \tag{3.3}$$

which is unity for a circular region and decreases with increasing ratio of perimeter to area, i.e., with increasing departure from a circular shape. Of 83 measured ordered phase domains we found $circularity = 0.41 \pm 0.13$.

We conclude that the ordered-phase domains created with specific adhesion do not represent equilibrated L_o–L_d lipid phase separation. Either adhesion has modified

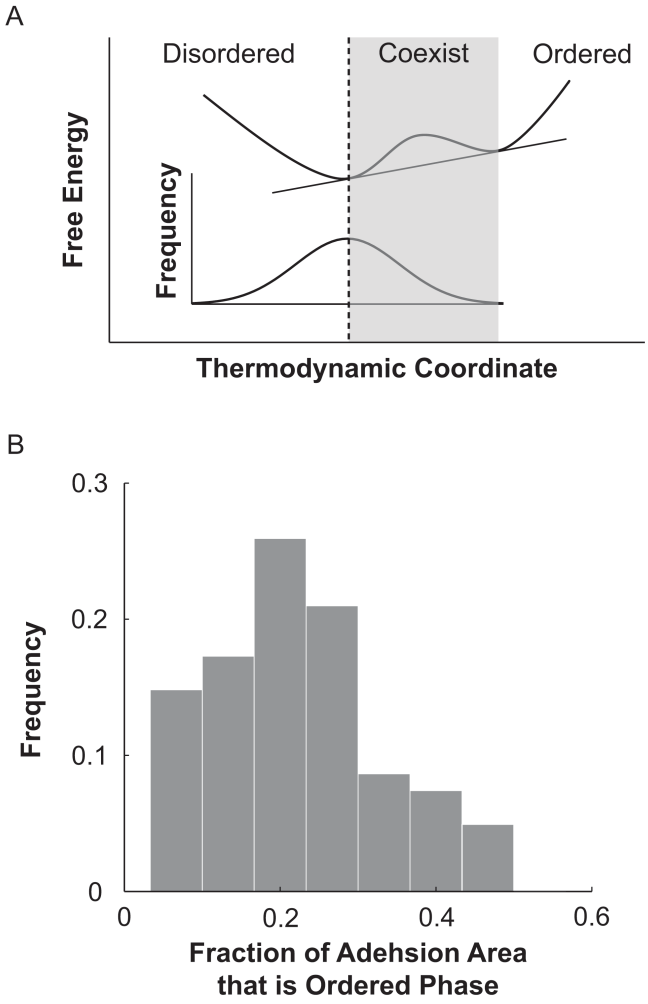

Figure 3.4: **For specifically-adhering GUVs that phase separate to form ordered-phase domains, the amount of ordered phase present is different than expected for free floating GUVs.** A) GUVs made by electroformation have a variable composition. We sketch the dependence of both the free energy (main plot) and the frequency (inset) of GUVs forming with a particular value of a thermodynamic coordinate determining if a vesicle will phase separate. Half of the GUVs phase separate (indicated by the greyed region; supported by experimental data in figure 1). In the coexistence region (grey shading), the likelihood of measuring a given fraction of ordered phase is a monotonically decreasing function. B) In contrast to the schematic in panel (A), the frequency distribution of 81 ordered-phase area fractions is roughly symmetric about an area fraction of 0.22±0.03. This histogram shows aggregated data for three experiments; data broken down by experiment is shown in Figure 3.5. The reported uncertainty is the standard error of the mean. (Adapted from [2]).

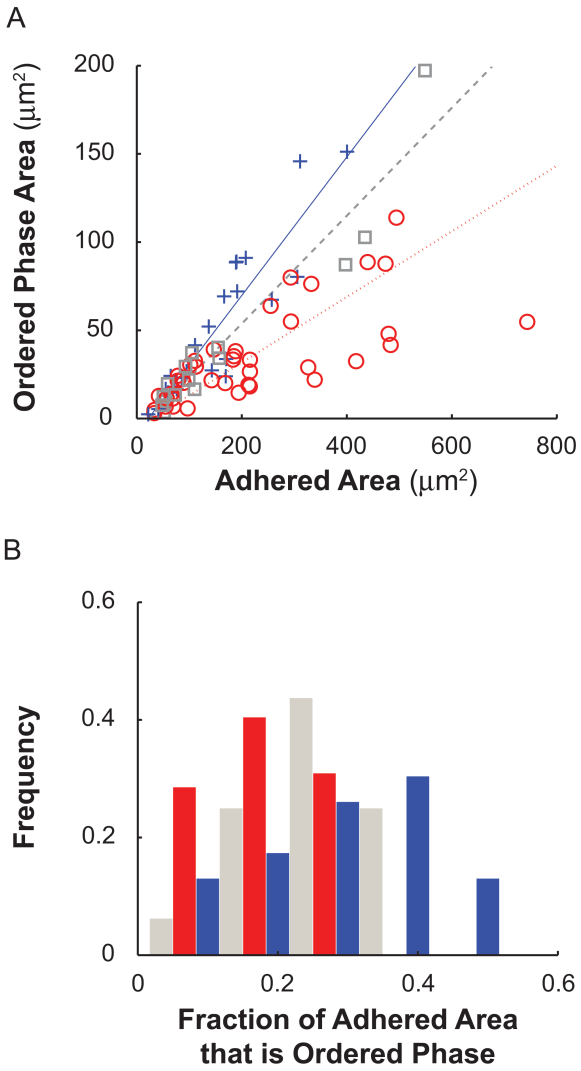

Figure 3.5: **For specifically-adhering GUVs that phase separate to form ordered-phase domains, the amount of ordered phase present is different than expected for free floating GUVs.** A) The area fraction of ordered phase in the adhering area is roughly constant. Shown are data points and linear fits for three separate experiments. Experiment 1: Blue crosses and solid-lined fit with a slope of 0.39 ± 0.08 and $R^2 > 0.82$; Experiment 2: Grey crosses and dashed-lined fit with a slope of 0.31 0.05 and $R^2 > 0.92$; Experiment 3: Red circles and dotted-lined fit with a slope of 0.19±0.02 and $R^2 > 0.88$. The reported uncertainties are the 95% confidence intervals. B) Shown are histograms of the ordered-phase area fractions of the adhering area for the same three experiments as in panel (A), coded by the same colours. In contrast to the schematic in Figure 3.4A, the frequency distribution of ordered-phase area fractions in each experiment show a non-monotonic dependence on area fraction. (Adapted from [2]).

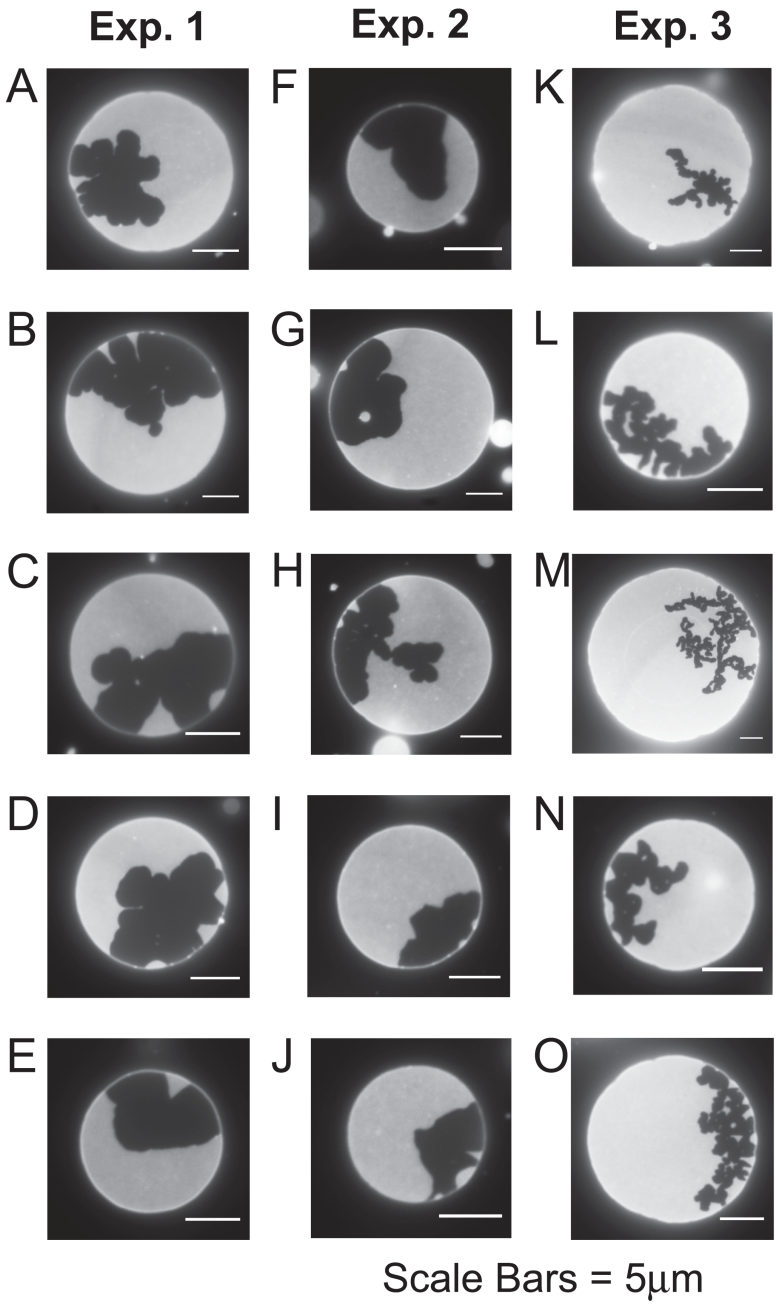

Figure 3.6: **For specifically-adhering GUVs that phase separate to form ordered-phase domains, the amount of ordered phase present is different than expected for free floating GUVs.** Catalogue of typical ordered domain shapes grouped by experiments numbered the same as in Figure 3.5. Experiment 1 (A-E), Experiment 2 (F-J); Experiment 3 (K-O). (Adapted from [2]).

the equilibrium phase behaviour of our membranes, or these membranes are out of thermodynamic equilibrium.

3.4.6 Ordered-phase domains exclude and are bounded by biotin-neutravidin binding proteins

To assess the role that biotin-neutravidin binders might play in keeping the membrane out of thermodynamic equilibrium by limiting the growth of ordered-phase domains and/or shaping non-circular domains, we adhered vesicles using Neutravidin that was conjugated with the fluorophore Oregon Green (neutravidin-488). Oregon Green is spectrally distinct from DiI, which allowed us to separately image the binding proteins and the disordered-phase membrane. In every specifically-adhering vesicle containing an ordered-phase domain, the fluorescent signal from the neutravidin-488 was excluded from the ordered-phase domain and appeared uniform in the disordered region (Figure 3.7 a, b, c). Conversely, every vesicle that did not phase separate displayed a uniform fluorescent signal from the neutravidin-488 throughout the adhesion region (Figure 3.7 d, e, f).

From this, we conclude the biotin-neutravidin binders are uniformly dense (to optical microscopy) in the disordered-phase portion of the adhering area and that binders are absent from the ordered-phase region. Moreover, we infer that the ordered phase excludes biotinylated lipids bound to neutravidin as impurities similar to its exclusion of the amphiphilic dye DiI.

Impurities, like our binders and dye, can be excluded from ordered lipid phases when their inclusion in the ordered phase costs more free energy than their exclusion to the disordered phase. This is specific to the chemical structure of the impurity and the molecular arrangement of the lipid phases involved [78]. Thus, partitioning of impurities is consistent with equilibrium physics. However binders can jam together and become immobilized; if the binders in the binder-rich, disordered-phase region are kinetically trapped, then our membranes' phase domains may not be in thermodynamic equilibrium.

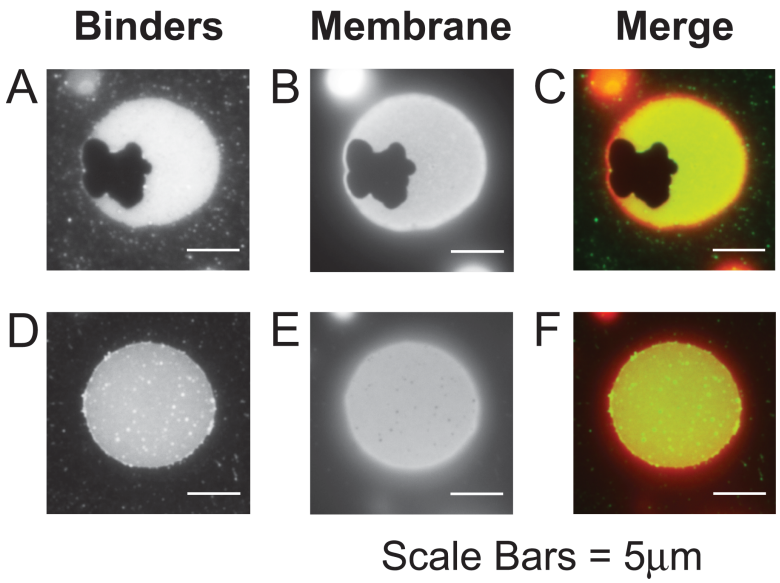

Figure 3.7: **Biotin-Neutravidin binders are excluded from ordered-phase domains and are uniformly distributed in adhering, disordered-phase regions.** Epifluorescent micrographs show, (A and D) fluorescently-labelled neutravidin (Oregon Green) and (B and E) the fluorescent disordered-phase marker DiI. These two spectrally-distinct channels are co-localized in both phase separated and non-phase separated vesicles as illustrated by false-colour merged images (C and F). Neutravidin is false-coloured green and DiI is false-coloured red. (Adapted from [2]).

3.4.7 The disordered-phase marker DiI is enriched in regions with binding proteins

It has recently been shown that GUV membranes containing the same components as ours, modulo the substitution of DiPhyPC for DOPC as the low-melting-temperature lipid, and streptavidin for neutravidin, will be enriched in the disordered-phase marker DiI in the adhesion zone if the membrane composition is near a critical point [89]. This enrichment has been attributed to a molecular affinity of the DiI dye, which is a two-tailed lipophile, for the hydrophobic tail regions of the biotinylated DOPE. Our membranes are not near a critical point. To determine whether the binder-containing regions of our membranes are also enriched in DiI, we followed the measurement tactic used in Zhou et al. [89] and found the ratio of the fluorescent intensity of DiI in the disordered-phase part of the adhesion region to the intensity of DiI at the top of the same vesicle, where the membrane is non-adhering: We quantified the circularity of

ordrered-phase domains using the measure

$$enrichment\,ratio = \frac{intensity\,in\,the\,adhered\,disordered\,phase\,region}{intensity\,in\,the\,nonadhered\,vesicle\,top} \tag{3.4}$$

This ratio will be greater than one if the adhering region is enriched in DiI.

We account for photobleaching effects by measuring two sets of adhering vesicles in opposite orders—adhering bottom first and top second, or else top first and bottom second. We found that imaging the bottom first produced enrichment measurements greater than if the top was imaged first, so we infer that photobleaching can have a pseudo-enhancing and pseudo-diminishing effect on our measurements. We interpret the geometric average of these two histograms as the approximate real enrichment ratio, which was 1.6 ± 0.2 (Figure 3.8a). This is similar to that found in Zhou et al. [89] and indicates that the disordered phase in specifically-adhering regions contains more DiI than does the disordered phase in the free membrane. When we made corresponding measurements on the bottom and top of sedimented vesicles, the real enrichment ratio was 1.0 ± 0.1 (Figure 3.8B), meaning that there is about the same amount of DiI in the top and bottom of sedimented vesicles.

It is striking that we find DiI enrichment resulting from adhesion in membranes that are not near a critical point, whereas Zhou et al. reported DiI enrichment only in proximity to a critical point, albeit in membranes using DiPhyPC as a low-melting lipid rather than DOPC [89] To check that our measurement techniques yielded results in agreement with Zhou et al. we made GUVs of the same critical composition [89] (30:20:50 DiPhyPC:DPPC:Cholesterol) and found enrichment similar to that reported previously. We also checked for enrichment in adhering vesicles made of 21.5:21.5:57 DPPC:DiPhyPC:Cholesterol, which phase separate at room temperature [79]. Again, we measured DiI enrichments in ordered-phase adhered regions similar to those found at the critical composition. When we use fluorescently-labelled neutravidin, we find that DiPhyPC-containing vesicles have the neutravidin fluorescent signal always and only co-localized with the DiI signal (Figure 3.9).

From these results we conclude that the disordered-phase regions in the adhesion zones are enriched in membrane dye relative to the non-adhered portion of the vesicle membrane; this enrichment effect is present in both phase-separated and non-phase-separated vesicles and is absent in non-adhered, sedimented vesicles.

It is evident that the interface between the GUV and the SLB is enriched in neutravidin compared with the rest of the SLB (Figure 3.7 A and D). Following

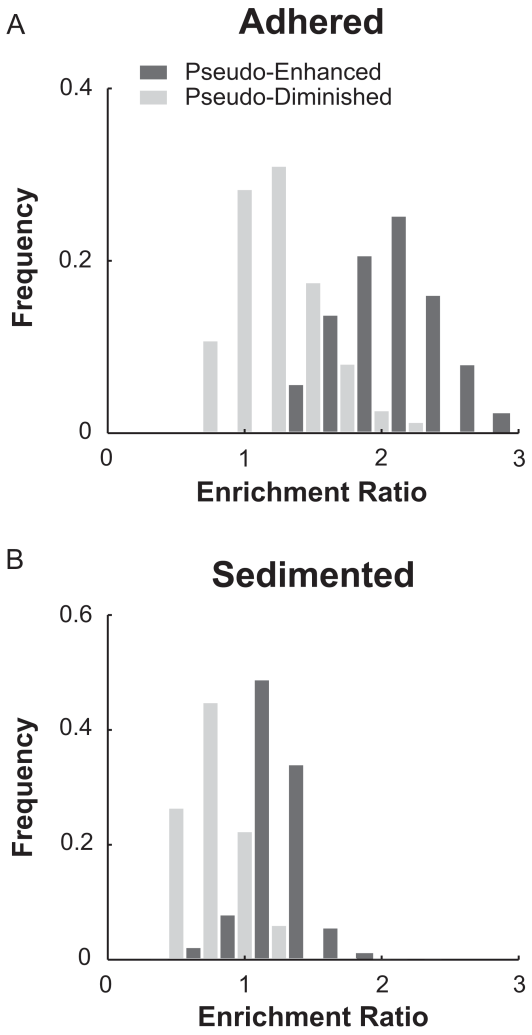

Figure 3.8: **Specific adhesion enriches the disordered-phase region of the adhering membrane in the membrane dye DiI.** Shown are histograms of the ratios of DiI intensity in the disordered-phase adhering region to DiI intensity at the non-adhering top of the membrane. Measuring an enrichment ratio greater than one indicates that the disordered-phase in the adhering region contains a higher density of DiI than the free membrane. To account for photobleaching resulting from fluorescence excitation, we imaged in two orders: bottom and then top resulted in pseudo-enhanced enrichment (dark grey bars); top and then bottom resulted in pseudo-diminished enrichment (light grey bars). A) In specifically-adhered vesicles the average enrichment measurement across the two data sets is 1.6±0.2; B) In sedimented vesicles the average enrichment measurement across the two data sets is 1.0±0.1. The reported errors are the standard deviations of the distributions. (Adapted from [2]).

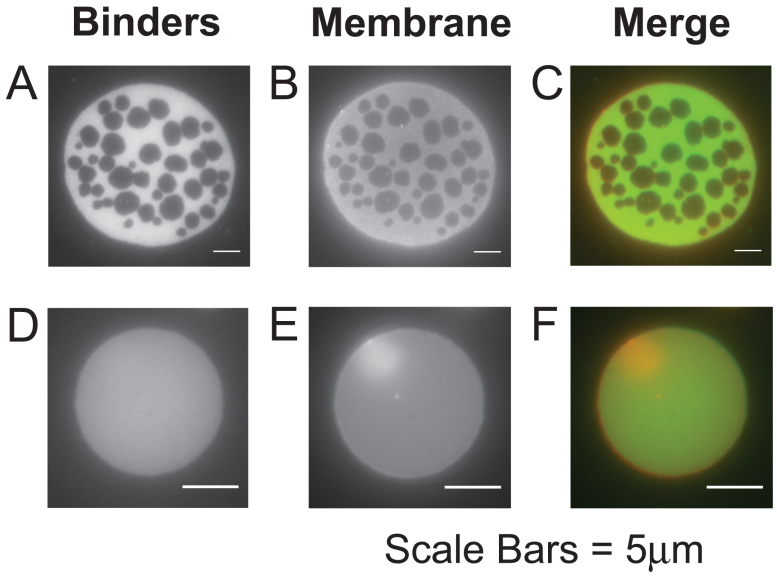

Figure 3.9: **Biotin-Neutravidin binders are excluded from ordered-phase domains and are uniformly distributed in adhering, disordered-phase regions in 21.5:21.5:57 DPPC:DiPhyPC:Cholesterol.** Epifluorescent micrographs show, (A and D) fluorescently-labelled neutravidin (Oregon Green) and (B and E) the fluorescent disordered-phase marker DiI. These two spectrally-distinct channels are co-localized in both phase separated and non-phase separated vesicles as illustrated by false-colour merged images (C and F). Neutravidin is false-coloured green and DiI is false-coloured red. (Adapted from [2]).

Zhou et al. [79], we attribute the enrichment of dye in the binder-rich portion of the adhering membrane with the molecular affinity of DiI for the tails of biotin-conjugated DOPE lipids. Assuming the DiI molecules are free to diffuse across the boundary between the adhered portion of the membrane and the non-adhered portion of the membrane, the dye enrichment in the adhesion zone is probably thermodynamically equilibrated.

3.4.8 Specific adhesion simultaneously supports dual heterogeneities in lipids and proteins

All our results taken together demonstrate that adhesion mediated by a single protein interaction results in the formation and stabilization of two types of coexisting domains: (1) an ordered-lipid phase that is enriched in the higher-melting lipid and

that excludes the DiI membrane dye and biotin-neutravidin binders; and (2) a disordered lipid phase that is enriched in the lower-melting lipid, the DiI membrane dye, and biotin-neutravidin binders. These heterogeneities may or may not be in thermodynamic equilibrium.

3.5 Discussion

The DPPC:DOPC:Cholesterol mixture that we have used in our experiments is known, at room temperature, to be near a coexistence region containing fluid-ordered (L_o) and fluid-disordered (L_d) lipid phases [76]. It was our expectation upon beginning these experiments that adhesion of homogeneous, L_d GUVs would result in the formation of circular L_o domains. However, the ordered-phase domains that we see are notably not circular and they do not change shape over the timescale of a day or with drastic increases in temperature. Therefore, the ordered-phase domains we see in adhering GUVs are not equilibrated LL_o domains, since the line tension at domain perimeters would make a circular Lo domain the lowest-energy shape for co-existing L_d–L_o phases. We suggest two possible, but not mutually exclusive, explanations for non-circular domains: (1) the ordered phase may be gel rather than liquid-ordered and/or (2) the binders are in a jammed state preventing the domains from equilibrating.

3.5.1 Explanation 1

Others have suggested that when a vesicle membrane is phase separated into L_o and L_d phases, increasing the membrane tension may change the ordered phase from liquid-ordered to gel; a mechanism for this has not been shown [84]. Our membranes are adhesively tensed. If increasing membrane tension causes the liquid-ordered phase to transition to a gel phase, the diffusion in the gel phase will be many orders of magnitude slower than in a liquid phase [163]. Very slow kinetics could effectively "freeze" the shape of the domain as it was when the gel formed so that no detectible changes happen over $\sim$24 hours of observation.

An alternative possible pathway for forming gel domains comes from the effect of adhesion on the free energy landscape of the GUV membranes. The free energy landscape of DPPC:DOPC:Cholesterol bilayers should contain a gel phase. At the

composition and temperature of our experiments, for non-adhered membranes the free energy of the gel phase should lie higher than the free energies of the L_d and L_o fluid phases. However, it could be formed as a metastable phase, as we have seen before for lipid membrane systems that undergo a rapid, deep quench by lowering temperature [78, 164]. In the present case, the quench would be a sudden decrease in entropy caused by adhesion, rather than a decrease in temperature.

Furthermore, the observation that adhesion favours the formation of ordered phases implies that adhesion will increase the free energy of softer phases more than it will increase the energy of stiffer phases [164]. Notably, this interpretation relies only on the empirical observation that adhesion favours the formation of ordered phases, and not on any inferred mechanism for how this works. If adhesion increases the free energy of the L_d and L_o fluid phases by similar amounts but leaves the free energy of the gel phase relatively unchanged, the common-tangent construction of the free energy versus composition curves could give an equilibrium coexistence between L_d and gel phases rather than L_d and L_o phases (Figure 3.10).

3.5.2 Explanation 2

Binding proteins may hinder the equilibration of lipid phase separation. Here we stress the correspondence between our work and that of Fenz et al, [40] who used the same specific-adhesion system that we do except that their GUV membranes were based on unitary SOPC bilayers rather than our ternary lipid bilayers. Those researchers mapped out how the states of protein distribution depend on the density of binders in the GUV and in the SLB and found that at high binder concentrations in the SLB, i.e., 0.5% or greater, the adhesion was complete and the adhesion zones were homogeneously dense in binding proteins [40]. However at low binder concentrations in the SLB, i.e., less than 0.5%, adhesion was incomplete and binding proteins were heterogeneously distributed in the adhesion zones. This was found to result in an annulus of high protein density surrounding a protein-free region (see Figures. 2 and 3 of Fenz et al.)[40] This annulus was attributed to jamming of the proteins; jamming is a non-equilibrium state.

In contrast, the biotin-neutravidin concentrations in our GUVs and SLBs, i.e., 1% in each, place us well into the complete-adhesion regime described in Fenz et al.)[40] In this regime, binding proteins are homogeneously distributed in the adhesion zone.

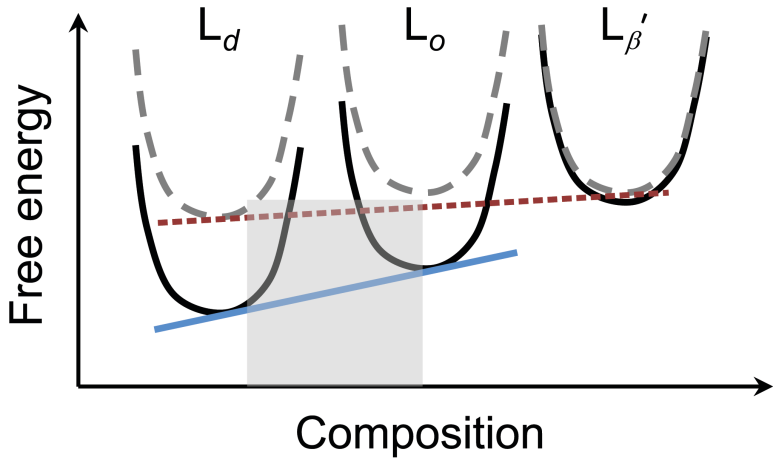

Figure 3.10: **Biotin-Neutravidin binders are excluded from ordered-phase domains and are uniformly distributed in adhering, disordered-phase regions in 21.5:21.5:57 DPPC:DiPhyPC:Cholesterol.** A speculative free-energy schematic showing how adhesion could change equilibrium phase coexistence by differentially raising the free energies of different lipid phases. The free energies of non-adhering membrane phases Ld, Lo, and Lb? are shown as solid black curves. Membranes with compositions indicated by the grey square will minimize free energy by phase separating into Ld and Lo phases, as indicated by the solid blue common tangent line. The free energies of adhering membrane phases are shown as dashed grey curves. The Lo phase has been raised 80% as much as the Ld phase and the Lb? phase has been raised 10% as much. Now, membranes with compositions indicated by the grey square will minimize free energy by phase separating into L_d and $L_{\beta'}$ phases, as indicated by the dotted red common tangent line.

However, the GUVs in Fenz et al. did not phase separate. We suggest that formation of an ordered phase that excludes binding proteins will exert a lateral pressure and jam binders into even higher concentrations. Jamming will prevent mobility of the binding proteins, which could provide a mechanical restriction that prevents the ordered-phase domains from rounding into circles.

Because biotinylated lipids have DOPE tails, and because the unsaturated DO tails will tend to be in the disordered phase, we surmise that binders may also prevent the area fraction of ordered lipid phase from growing to completion, as discussed for Figure 3.4 . Once the binder density in the adhered region is high, we do not know the degree of lipid-compositional coupling between the adhered and free portions of the same membrane. However, since the fraction of each GUV that is adhered

is constant, whether or not the adhered region is compositionally coupled with the non-adhered membrane should not change our equilibrium expectations, based on the lever rule. We suggest that the variation in ordered-phase area fractions that we measure (Figure 3.4B) may arise from variable kinetics of binder jamming competing with lipid phase separation and preventing lipid phase separation from maturing to equilibrium during adhesion.

3.5.3 Relationship of patterns in phase separated, adhered membranes to living cells

When living immune cells, T-Cells and B-Cells, adhere to a target they form a stable structure called the immunological synapse that is required for immunity-associated functions [154, 155, 156].

The spatial organization of the mature immunological synapse consists of concentric regions: a central region which is rich in ordered-phase lipids and TCR/MHCp binding complexes preferential to the ordered phase, and a peripheral region rich in disordered-phase lipids and LFA-1/ICAM-1 binding complexes preferential to the disordered phase. The TCR/MHCp binding complex gives an intermembrane separation of $\sim$15nm and the LFA-1/ICAM-1 gives an intermembrane separation of $\sim$40 nm [157]. What interactions give rise to the structure of the immunological synapse is unknown. Theoretical models that combine protein reaction kinetics with the free energy of a fluid lipid membrane can lead to stable heterogeneities in protein distributions in the immunological synapse [158, 165, 166, 167]. Having binders of two different sizes was essential for these models to produce stable heterogeneities; binder size impacted the dependence of association kinetics on intermembrane distance and it gave rise to a membrane bending energy cost when unlike complexes were next to each other. These models did not incorporate heterogeneities in lipid distribution or phase.

The topological characteristics of phase separation in our reductionist model system are very nearly those of the immune synapse, with a few exceptions. Our GUVs are made without proteins that are preferential for the ordered phase, and the binder densities in our system are much higher than those in immunological synapses. Most notably, and unlike previous reductionist descriptions, [158, 165, 166, 167] we have only one type of binding complex and our GUV membranes are made of a mixture

of lipids that can phase separate. Our results show that adhesion itself, even in a highly-reductionist system with only one species of binding complex and only three lipid species, may interplay with lipid phase separation to give rise to nested, dual heterogeneities if the membrane is sufficiently near a phase transition. This suggests that the many different interactions possible for the biological system, resulting from multiple types of binding complexes, cytoskeletal transport,[168] and much greater multiplicity of lipid species, may have greater fine-tuning power than previously suspected.

3.6 Conclusions

The broad goal of biophysical work on artificial and plasma membrane vesicles is to gain physical insight into the mechanisms driving organization in real cells' membranes. Our work has uncovered an effect leading to heterogeneities at the adhesion site of an artificial two-membrane junction. We show that a single type of adhesive interaction can simultaneously stabilize two types of heterogeneity in membrane protein and lipid composition. The resulting heterogeneities are robust against changes in temperature and represent long-lived non-equilibrium states.

Chapter Four: On a Nonequilibrium Fingering Pattern in Adhered Lipid Membranes

4.1 Abstract

We report on an experimental demonstration and theoretical description of a nonequilibirum dynamic pattern that occurs in microscopic lipid membranes adhered together by proteins. Using confocal fluorescence microscopy, we record time series of a dynamic fingering patterns occuring in a $\sim$25 μm diameter circular lipid membranes adhered by proteins to a lower surface supported lipid membrane. The fingers are $\sim\mu$m-scale pores that grow on the scale of 10s of seconds at the interface between an already stabilized hole in the upper circular membrane. We show theoretically that the evolution of these patterns are governed by a free energy which undergoes a saddle-node bifurcation during pattern formation at which point the process stops and remains at rest. Our model predicts that the rate of finger formation scales exponentially with the density of adhesion proteins and the size of formed fingers scales linearly with the density of adhesion proteins. We show that our experimental data matches these expectations.

4.2 Introduction

Living cells dynamically organize the components of their membranes into stably persisting functional structures. One example is provided by the T-cell when it forms an immunological synapse upon adhesion [154]. The T-cell's synapse, which is dynamic on the scale of several minutes and then static for 10s of minutes, has been the focus of numerous experimental and theoretical studies [158, 166, 167, 169]. Almost all of these studies use as a description, in some combination, the mobility of individual proteins, their binding rates, and the thermal undulations of elastic membranes.

In this Chapter, we present our experimental system, which is a minimalist membrane model for adhered cell membranes. It is constructed from materials—lipids and proteins—that are similar to those in eukaryotic cell membranes. The time and

length scales of the patterns we observe—micron-scale structures dynamically formed over tens of minutes—are similar to those that occur in living cells. Therefore, the pattern forming dynamics obtained in this system may be a step toward learning how pattern forming dynamics arise in real cell systems like the T-cell's immunological synapse. We offer a theoretical description of the dynamics of our experiments, which, in the spirit of phenomenological theories of phase transitions, overlooks the complexity of protein and membrane interactions. Therefore, in our description some degree of generality arises, which could also lend insight into real cellular processes.

In our experiments, we adhere a giant unilamellar vesicle (GUV) to a planar supported lipid bilayer (SLB) membrane using biotin-avidin binding. Once a GUV is stably adhered to the surface, we induce it to rupture so that a hole opens in the adhered region of the GUV. The interface boundary between the hole and the protein-bound membrane then grows in a complicated pattern where finger-shaped holes invade the protein-bound membrane. We track the evolution of the interface using confocal fluorescence microscopy. From our data we extract two growth laws, one for the width of the growing fingers and another for the rate of finger formation. Both growth laws are functions of an effective protein-bound membrane density and are derived from a phenomenological free energy function.

4.3 Experiment

We prepare GUVs composed of 87% DOPC, 10% Cholesterol, and 3% DOPE in 280 mM sucrose solution using electroformation. The GUVs are placed into a sample chamber filled with 280 mM PBS buffer solution with a SLB composed of 97% DOPC and 2% DOPE. For both GUVs and SLBs, we used DOPE which had the PE headgroup capped with biotin (DOPE-biotin). The SLBs were functionalized by binding neutravidin fluorescently-labeled with Atto-488 dye to the DOPE-biotin. When the GUVs settle to the bottom of the chamber they adhere to the SLB by biotin-avidin binding (left-hand side of Figure 4.1 and Figure 4.2A).

Once the GUVs are fully adhered, ultrapure water is allowed to seep slowly through a 0.4 μm polycarbonate membrane placed on the top of the rubber gasket, indicated schematically on the right-hand side of Figure 4.1. This adjusts the osmotic pressure across the GUV causing water to flow in and tense the GUV. Even-

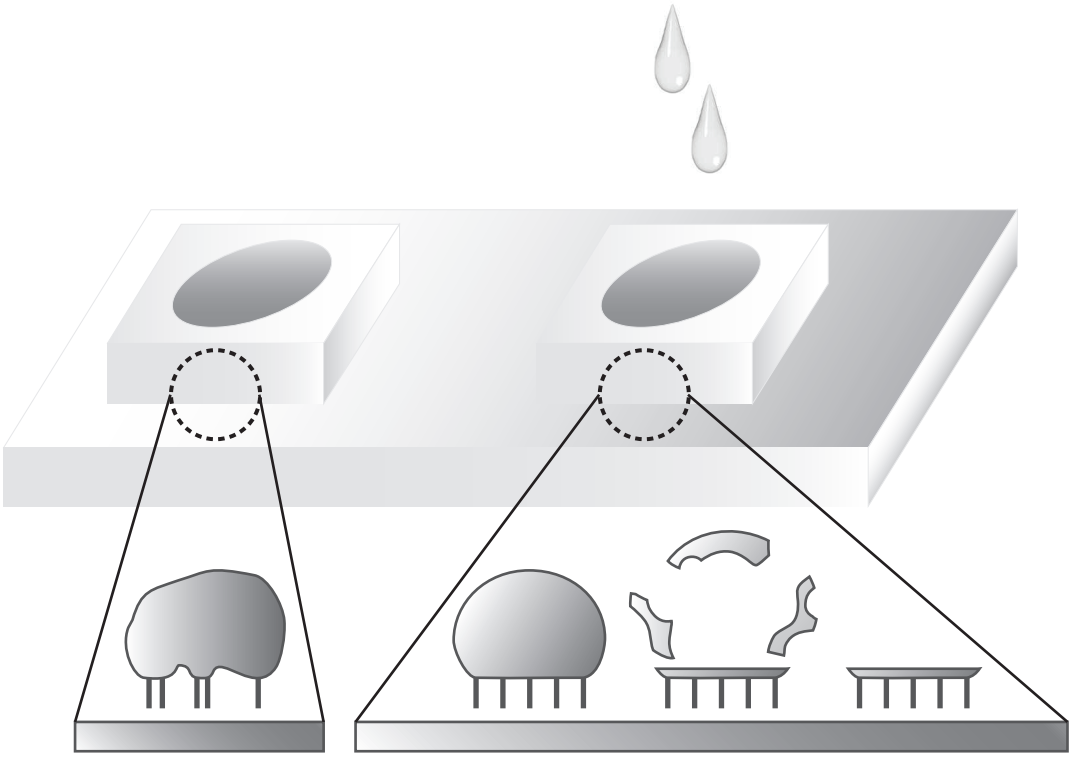

Figure 4.1: **Sketch of experimental setup.** Samples are formed in square rubber gaskets placed on a microscope coverglass. On the left-hand side of the sketch, an initially flaccid GUV is adhered to an SLB. The GUV contains 280 mM sucrose solution and the surrounding solution is 280 mM PBS. On the right-hand side of the sketch, ultra-pure Milli-Q water is slowly added to the surrounding solution, which reduces the osmolarity of the external solution and causes water to flow into the GUV. First the GUV tenses and then the GUV ruptures. After the GUV ruptures, all that remains of the GUV is the portion attached to the SLB

tually the GUV lyses leaving behind only the portion of the GUV that is adhered to the SLB by the biotin-avidin bonds.

In Figure 4.2, an initially flaccid vesicle (4.2A), is slowly tensed. After 500s (Figure 4.2B) the edge of the adhesion zone has moved inward leaving behind a dark halo where fluorescently-labeled protein initially aggregated on the SLB surface has been pulled inward by the contracting area of the adhered GUV. In Figure 4.1C, after 800 s, the GUV ruptures and a bright ring of immobile proteins becomes visible.

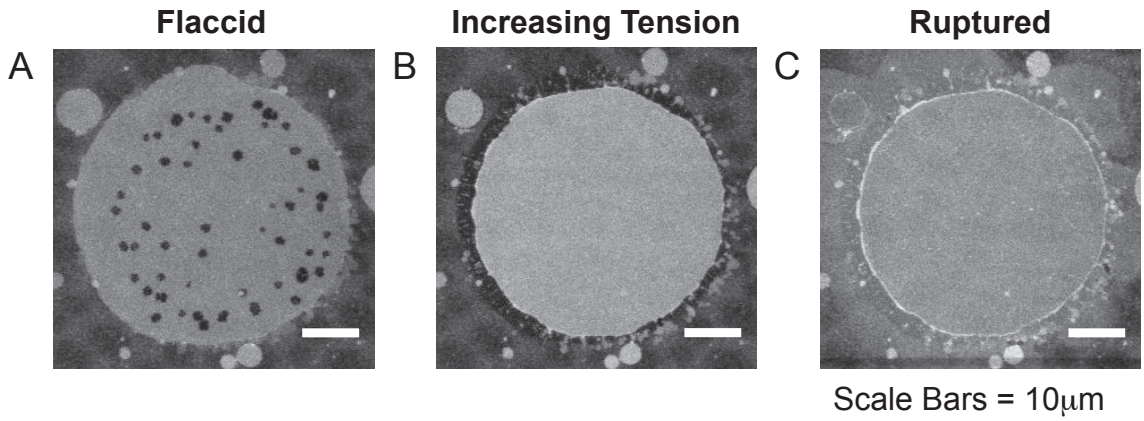

Figure 4.2: **Time series of experimental setup.** Confocal fluorescence micrographs of fluorescently-labeled neutravidin adhering a GUV to an SLB. In A, an initially flaccid GUV is adhered to the surface. The black spots in the adhesion zone are portions of the GUV that are buckled out-of-plane. Ultra-pure water is allowed to seep slowly into the the GUV. In B, after 500s, the GUV has tensed and the adhesion zone has contracted. Finally after 800s, in C, the GUV ruptures, leaving behind the adhered remnant.

4.3.1 Fingering

When an adhered GUV ruptures, holes may form in the membrane interior to the protein rim (Figure 4.3A). It is not *a priori* obvious that the fingers are holes in the membrane. In the next section, we use two different microscopy methods to indicate that the fingers are indeed holes.

After the tears in the adhered membrane form, they begin to grow in a finger pattern and invade the protein-bound membrane, which in turn becomes denser. Figure 4.3B shows an intermediate pattern at 200 s where some regions that have become isolated are visibly denser (e.g., the top rim and the two islands on the left) than the other parts of the membrane (e.g., the central region). In Figure 4.3C, after 400 s, the fingering pattern has arrested.

As the fingering pattern proceeds and the density of the protein binders increases, the size of the fingers decreases as does the rate at which the fingers form. These differences are evident in Figure 4.3: two micrographs of the fingering pattern, one at 200 s (4.3A) and one at 250 s (4.3B) are shown. In 4.3C the fingering pattern at 200s is false colored red and overlayed with the fingering pattern at 250s false colored in green. The places that the membrane was intact at 200s but was no longer at 250s,

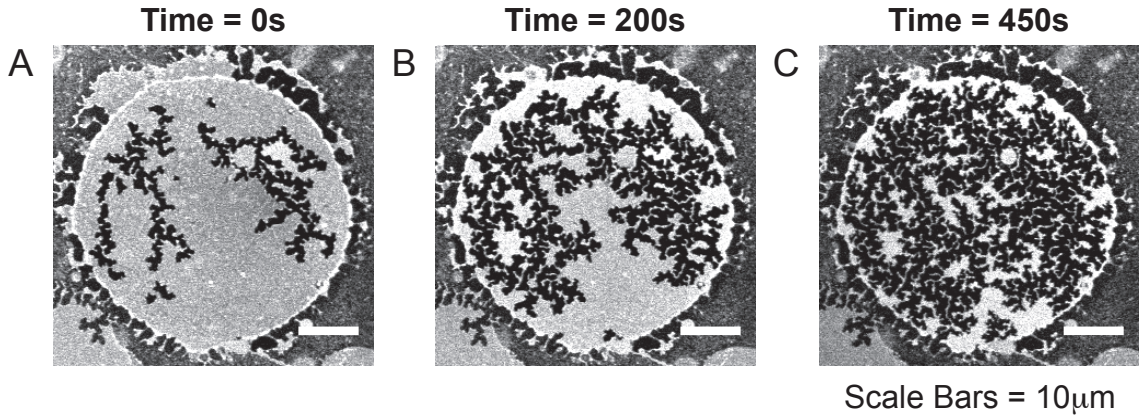

Figure 4.3: **Fingering pattern in an adhered membrane.** Confocal fluorescence micrographs of fluorescently-labeled adhesion proteins. In A an initial finger-shaped tear has appeared in the membrane. In B an intermediate fingering state at 200 s. In C the final, fully developed pattern at 450 s.

appear as red fingers. The denser regions,(e.g., the top rim and islands on the left) have smaller fingers with fewer formed per length than the less dense regions (e.g., the bottom portion).

4.3.1.1 Analysis

For the purpose of analysis we make three assumptions. First, we assume that the density of the protein-bound membrane in the final stage, as in Figure 4.3C, is the same in all intact parts of the membrane. Second, we assume that the density of proteins in the fingers is zero. Finally, we assume that the total number of binding proteins is conserved during the duration of the finger forming process. Under these assumptions we can track the decrease in density of each region of the membrane backward in time from the final state as the pattern evolved. For example, we identified 23 regions of 4.3C that the fingers failed to fully invade. As time moved backward, those regions got larger and collected proteins. When two regions merged, they became one region. We carried out this procedure until all the regions coalesced and thus we determined the density of every region of the pattern displayed in Figure 4.3 at each time point.

Since we don't have a direct measure of the absolute number of proteins in a given membrane, we define the final density of a fully formed pattern to be unity and define

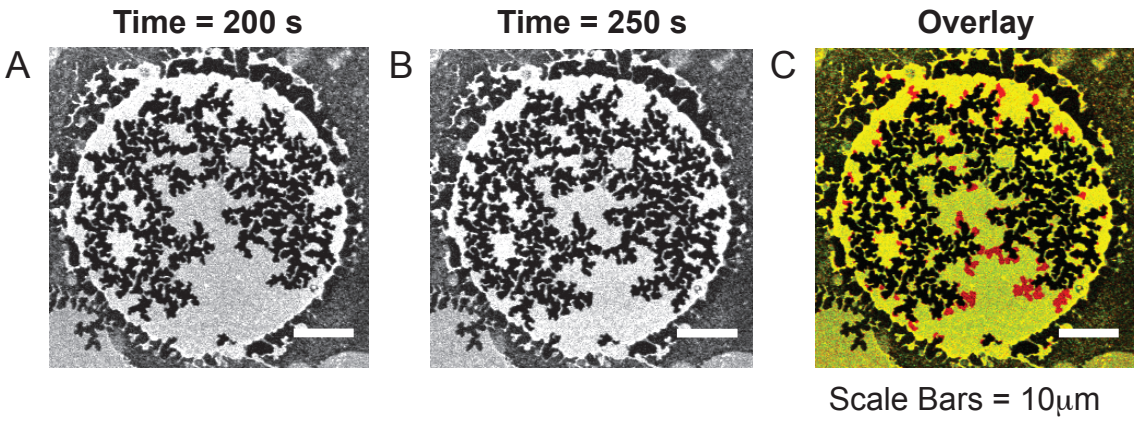

Figure 4.4: **Density dependence of fingering.** Confocal fluorescence micrographs. In A an intermediate state at 200s is shown, some regions (e.g., the top rim and two islands on the left) are brighter than others (e.g., bottom and central regions) because the fluorescently-labeled avidin is denser. In B a later intermediate state at 250s is shown. In C, the two images are false colored and overlayed (200s in red and 250s in green). The overlay displays the fingers that grew between 200s and 250s in bright red. Inspecting the red fingers indicates that fingers grow smaller and with less frequency in denser regions.

lesser densities relative to the final density. From our data we could measure the width of the fingers that invaded a region with a given density, and we could measure the number for fingers that formed per unit length per unit time that formed at the boundary of a region with a given density. These measures are discussed below in the Theory section.

4.3.2 Evidence That Fingers are Holes

Our experiment is, to our knowledge, the first reported case of dynamic pores forming at the interface between protein-adhered lipid membranes. Although, the lipid composition of our membranes is anticipated to be miscible at all temperatures [76], we nevertheless make two distinct measurements separately indicating the fingers are holes rather than a lipid phase that excludes protein binders and the membrane dye DiI. (When membranes containing the disordered phase dye DiI undergo fingering, the DiI signal is absent in the fingers, e.g., Figure 4.6B)

4.3.2.1 Fluorescence Evidence

We conducted a control experiment by adhering GUVs composed of 33.5% DOPC, 33.5% DPPC, 30% Cholesterol, and 3% DOPE-biotin to a SLB of same composition discussed above. This GUV composition is anticipated to exhibit coexisting liquid ordered and liquid disordered phases at room temperature [76]. The adhered GUVs also formed fingers in the protein-adhered region. Thus, we could compare phase separation in the free portion with fingers formed in the adhered portion.

We treated the adhered vesicles with the fluorescent dye laurdan that dissolves in both disordered and ordered phases. The emission spectrum of laurdan depends on which phase it is in [170]. In the disordered phase, the laurdan emission spectrum is peaked at 490 nm and in the ordered phase, the peak is lower (for gel phases the peak is at 445nm). We used two-photon microscopy in the typical way as follows. After, treating our sample with laurdan dye, we excited it with a 780nm laser which excited the dye *via* two-photon absorption. The emission spectrum of the dye was collected simultaneously through two channels, 445nm and 490nm. Using the intensity in the 445nm channel, I_{445}, and the intensity in the 490nm channel, I_{490}, we calculated the generalized polarization [170]

$$GP = \frac{I_{445} - I_{490}}{I_{445} + I_{490}} \tag{4.1}$$

If laurdan is located in a ordered phase $GP > 0$ but if it is located in a disordered phase $GP < 0$. We found that in the phase separated free portion of the membrane Figure 4.5A and 4.5B, the GP confirmed the existence of an ordered phase indicated in red in Figure 4.5C. However, in the adhered portion of the GUV that formed fingers, although the laurdan signal was present, Figure 4.5 D and E, the GP measure failed to indicate the existence of an ordered phase.

4.3.2.2 Reflection Evidence

We used confocal reflection microscopy in conjunction with confocal fluorescence microscopy as a second method to determine whether the fingers in our membranes were holes. We adhered GUVs composed of 87% DOPC, 10% Cholesterol, and 3% DOPE-biotin to an SLB the same as previously discussed. We incorporated the fluorescent dye DiI into the GUV and used neutravidin fluorescently-labeled with Atto-488 dye.

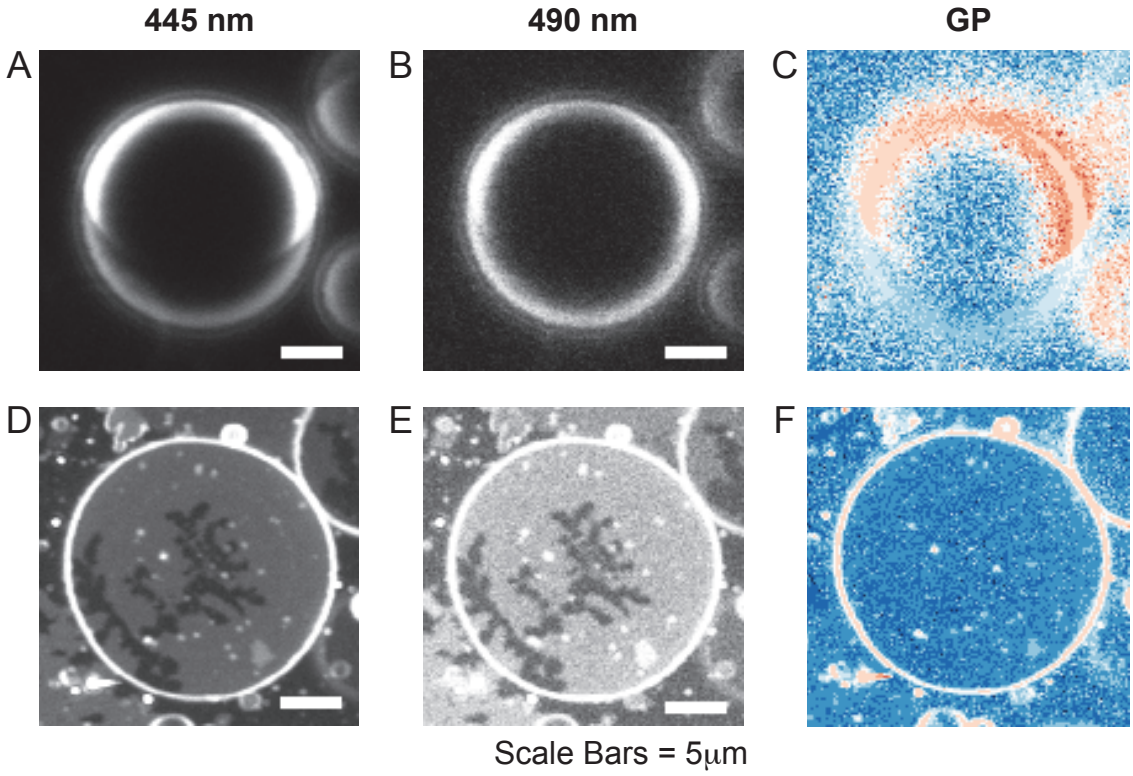

Figure 4.5: **Fluorescence evidence that fingers are holes.** Two-photon fluorescence micrographs in A, B, D, E. In A and B the laurdan signal from the free portion of the adhered membrane yields a genearlized polarization in C that indicates the coexistence of ordered and disordered lipid phases. In D and E the laurdan signal from the adhered portion of the membrane that exhibits fingers, yields a generalized polarization in F that fails to indicate the fingers are an ordered lipid phase.

DiI and Atto-488 can be imaged separately with red emission (560nm-660nm) and green emission (505nm-525nm) filters respectively.

In our experiment, we expected both DiI and Atto-488 to be absent in the fingers, however, if the fingers were an intact membrane rather than a hole, we expected they would reflect the light from the 488nm confocal laser. The results are shown in Figure 4.6. In 4.6A and 4.6B the fluorescence signal indicated the absence of disordered phase and adhesion proteins in the fingers, as expected. However, Figure 4.6C indicates that the fingers failed to reflect the confocal laser.

Taking the fluorescence and reflection data together, which failed to indicate the fingers were membrane, along with the fact that the composition of GUVs in our

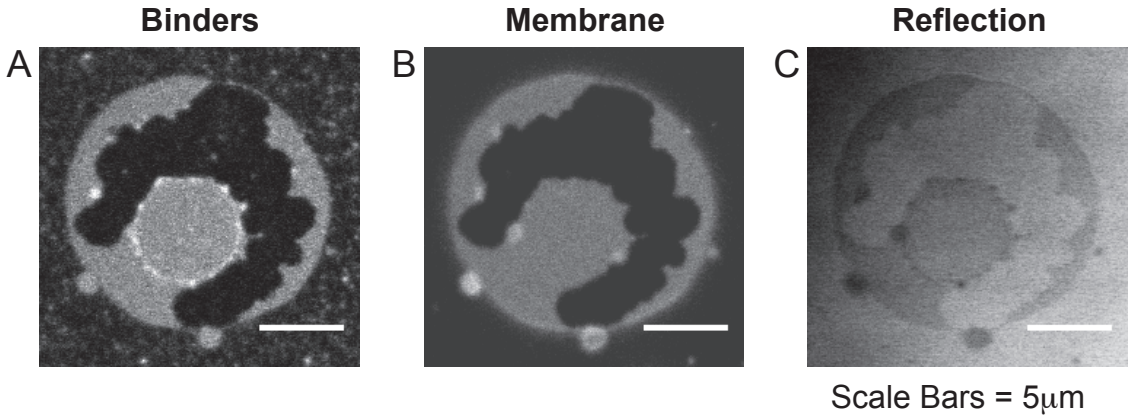

Figure 4.6: **Reflection evidence that fingers are holes.** Confocal fluorescence and reflection micrographs. In A, the 488-fluorescently-labeled neutravidin is excluced from the fingers. In B, the membrane dye DiI is excluded from the fingers. In C, the fingers fail to reflect the confocal laser.

experiments are supposed to be miscible at all temperatures, leads us to assume that the fingers are indeed holes in the adhered membrane.

4.4 Theory

We model the dynamics of the finger-shaped holes in our membrane by treating the fingers as tension-induced membrane pores forming at the interface between an already existing membrane hole and the protein-bound membrane. A usual starting point for a theory of tension induced pore formation in fluid membranes [171] is with a free energy function F of a circular pore with radius R that has the form

$$F(R) = 2\pi\Gamma R - \pi\Sigma R^2 \tag{4.2}$$

The quantity Γ is line tension along the edge of the pore and Σ is the surface tension jump across the pore boundary. The intuitive picture is that increasing R decreases the surface free energy $-\pi\Sigma R^2$, which favors pore formation, but increases the boundary energy $2\pi\Gamma R$, which disfavors pore formation. The free energy F exhibits a maximum of $F^* = \pi\Gamma^2/\Sigma$ when the radius R is equal to $R^* = \Gamma/\Sigma$. If a local fluctuation of free energy occurs that exceeds F^*, then a pore will form and grow unbounded. The usefulness of the simple free energy landscape given by Equation 4.2

is that the free energy maximum F^* depends on the simple quantities Σ and Γ, which have been measured [172]. Since the rate of pore formation depends on F^*, measuring this rate can be related to standard experiments [171]. We find it necessary to modify the free energy of pore formation to be amenable to our finger-forming process.

In typical pore-forming experiments with GUVs, one of two outcomes occurs: either a temporarily stable pore forms and allows fluid to escape, thus reducing tension in the GUV and causing the pore to close [173]; or else the vesicle is annihilated, as when it is aspirated into a micropipette [174]. In our experiments with surface-stabilized membranes, two regions, a membrane hole absent of protein binders and a protein-bound membrane, coexist side-by-side with an interface between them. There is capillary pressure across the interface and there is line tension along the interface. Thus, if a free energy fluctuation exceeds some threshold value $\mathcal{F}^*$, then a pore forms at the interface. Once a pore forms, it grows in size invading the protein-bound membrane region, which has some density ρ. At a certain point, the growth of the pore arrests and what remains is a stable finger of a certain width λ and a protein-bound membrane of density $\rho' > \rho$. After a time, a fluctuation $\mathcal{F}^{*\prime} > \mathcal{F}^*$ will occur at the boundary and form a finger, which then grows to a certain size $\lambda' < \lambda$. This process will continue until the protein-bound membrane reaches a final density ρ_f and the last fingers to grow are of the smallest width λ_f.

We model the fingering process by treating the fingers as pores that form along the boundary between already formed fingers and the protein-bound membrane. Once the fingers form, they grow as semicircles and relax the tension in the membrane. Thus, we assume the formation of a finger with width $r \geq 0$ is governed by the free energy [173],

$$\mathcal{F}(r) = -\sigma\left(1 - \frac{r^2}{r_0^2}\right) r^2 + \gamma r \tag{4.3}$$

In Equation 4.3, $\sigma(\rho)$ is the net tension in the membrane and is a monotone decreasing function of ρ, γ is the constant line tension of the finger boundary, and r_0 is the width at which the tension vanishes. As σ diminishes with increasing ρ, the energy barrier $\mathcal{F}^*$ increases and λ, the final finger width, decreases. We assume both $\mathcal{F}^*$ and λ can be Taylor expanded as functions of ρ. First, we assume $\lambda \approx \lambda_f + \beta(1-\rho)$. We can extract λ_f and β from our experimental data. Figure 4.7 shows λ plotted versus $1 - \rho$. The result is $\lambda_f = 0.27 \pm 0.04\mu$m and $\beta = 1.0 \pm 0.1\mu$m.

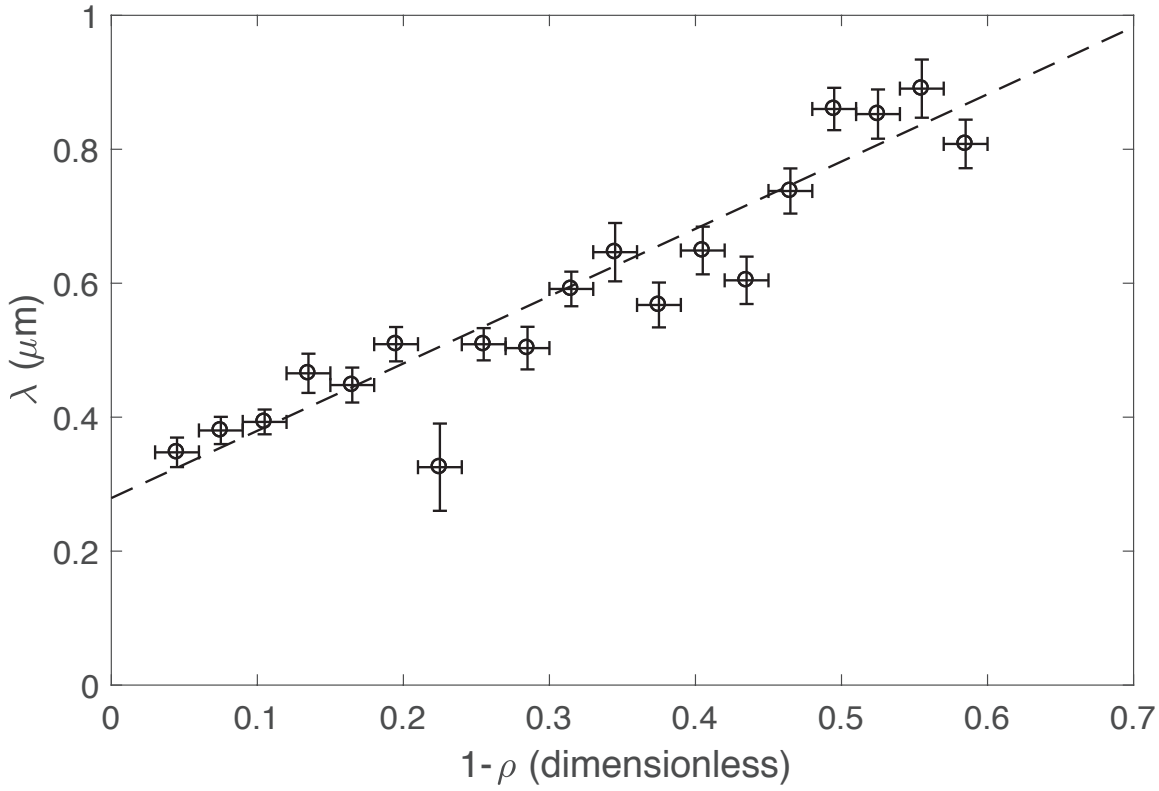

Figure 4.7: **Finger width versus density.** The width of the growing fingers depends linearly on the density. 524 measurements of finger widths were binned by density into 20 groups. The error bars in density are the half width of the bins (0.015) and errors in the finger widths are the standard errors of the mean finger width in each bin.

In order for a finger to form, a free energy fluctuation the size of $\mathcal{F}^* \approx \mathcal{F}_0^*(1-\rho)$ must occur at the interface between a hole and the protein-bound membrane. For a given boundary length L, time interval Δt, and density ρ, the number of fingers N that form per unit length per unit time, will follow an Arrenhius rate law. Thus, from our data, we fit

$$\frac{N}{L\Delta t} = Ae^{\mathcal{F}_0^*(1-\rho)} \tag{4.4}$$

The results of this fit, shown in Figure 4.8, are $\mathcal{F}_0^* = 3.8 \pm 0.8$kT, and $A = 0.0035 \pm 0.0010$ μm^{-1}s^{-1}.

We can compare our results to what others have found in free floating GUVs. For $\rho = 0.5$, which roughly corresponds to the initial state of the membrane just after

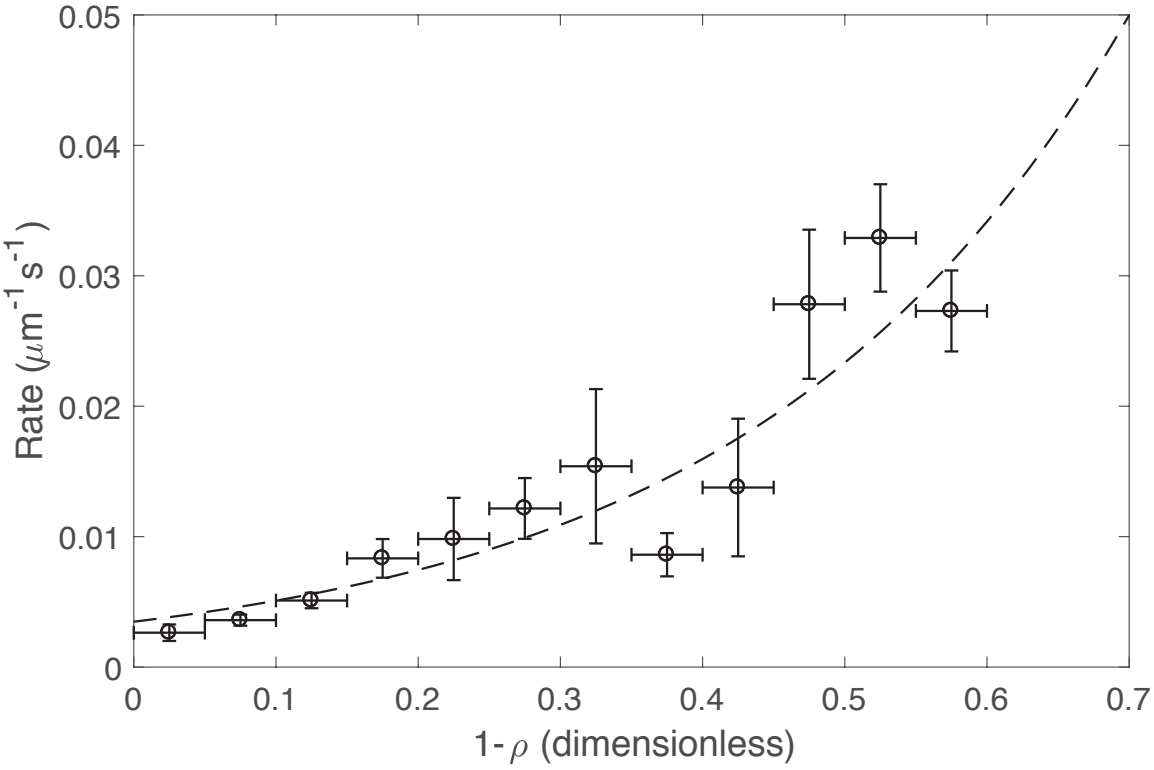

Figure 4.8: **Finger formation rate versus density.** The rate of finger formation depends exponentially on the density. 173 measurements of finger growth rates were binned by density into 12 groups. The error bars in density are the half width of the bins (0.025) and error in finger width is the standard error of the mean finger formation rate in each bin.

tearing, we have an activation energy $U_{0.5} = \mathcal{F}^*(0.5) \approx 2$kT. On the other hand for $\rho = 0.9$ we have $U_{0.9} = \mathcal{F}^*(0.9) \approx 3.5$kT. We must compare our activation energy with the energy required to form a semicircular pore of radius R at a boundary with an initial line energy $2\Gamma R$. If $U_a = \pi\Gamma^2/\Sigma$ for a circular pore, then forming a semicircular pore requires an activation energy $U_a' = (1/2)((\pi-2)/\pi)^2 U_a$. Thus, with $F^* \approx 20$kT [175], $U_a' \approx 1.5$ kT. In our adhered membranes, then, the activation energies range from 1.5 to 3 times that in a non-adhered GUV.

4.5 Conclusion

We have presented our experimental pattern forming model membrane system that exhibits time and length scales observed in living cells. We developed a phenomenological theory based on the thermal theory of tension induced pore formation. We demonstrated that analysis of our experiment matches the expectations of the theory. And we have compared our results with what others have done and found our results are consistent.

Chapter Five: Summary and Outlook

We began this dissertation by reviewing the field of experimental membrane biophysics within the context of biological systems. In Chapter 2 we argued that despite the successes of previous experimental studies, there remains much to be done if experimental systems are to yield phenomena nearer to those observed in living cells. Toward that end, we synthesized disparate experimental systems into a single system. Our study extended the range of experimental results to include a dynamic pattern-forming process occurring at the adhesion zone where membrane vesicles are bound to a planar membrane supported on glass *via* biotin-avidin binding.

The experiments other researchers have conducted have focused on mimicking certain aspects of organization in the plasma membrane of living cells. In particular, two classes of experiments have been traditionally pursued. One class, lipid phase separation, has been extensively studied at thermodynamic equilibrium [75, 76], and more recently, the dynamics of lipid phase separation have been measured [80]. A similar path has been taken in experiments studying the adhesion of membranes by proteins. Lateral heterogeneity in binding proteins has been attained in equilibrium situations [40, 60, 62], though sometimes the proteins form amorphous clusters which are immobile but not thermally equilibrated. So too has the dynamics of protein mediated adhesion been explored [42, 48, 61].

Our first experimental goal was to combine lipid phase separation with protein adhesion. Based on previous work on mixed lipid membranes adhering above their miscibility transition temperature *via* nonspecific physical interactions [85], we expected mixed lipid membranes adhered by proteins would phase separate above their miscibility transition temperature. What we found did not match our expectations. Instead our system exhibited large, $\sim 5-10\,\mu$m, holes that were stabilized at the adhesion interface between vesicles and solid supported membranes. The experimental signature that these stable holes were formed was very similar to what we supposed the experimental signature for lipid phase separation would have been. We incorporated the fluorescent dye DiI into our membranes which is known to partition away from ordered-phase domains. Thus, a membrane that formed an ordered-phase domain in the adhesion region would have a region where the DiI was absent and hence

the region would appear dark in a fluorescence image. However, so too would a hole in the membrane appear dark. To verify we observed the latter rather than the former, we reported three sets of measurements, which, in distinct ways, indicated the dark domains we observed where holes rather than ordered phase domains.

First, we used confocal fluorescence microscopy to measure the geometric characteristics of adhered vesicles by reconstructing their three dimensional shapes. In particular, we compared the volume V contained within an adhered vesicle, to the volume that would be contained within a sphere that had a vesicle's surface area A. Since all this vesicles were spherical before they adhered, this is a way to measure the volume change associated with adhesion and with patterning. To accomplish this we used the dimensionless measure $6\sqrt{\pi}V/A^{3/2}$ and compared vesicles that did and did not exhibit dark domains. We found that patterned vesicles, i.e., those with dark domains, retained 84% of the volume enclosed in an equal area sphere while non-patterned membranes retained 98%. This suggested the transition from non-patterned to patterned membranes involved a loss of internal volume. Since the osmotic pressure across the membrane initially balanced the Laplace tension in the membrane, a loss of internal volume means a pore must have opened at some point to release internal volume within. In our experiments we observe that dark domains first appear near the adhesion region in the free, non-adhered portion of adhered membranes. After a dark domain forms, the adhered membrane loses internal volume and, as more biotin-avidin bonds are created, the free portion of the adhered membrane is pulled onto the surface. The dark domain is pulled onto the surface along with the free portion of the membrane. Once a dark domain is completely enclosed by protein binders in the adhesion region, the process of the free portion of the membrane being pulled to the surface stops. These observations are consistent with the dark domain being a hole in the membrane through which internal volume is released until the hole is completely surrounded by protein binders in the adhesion region.

Second, we conducted a control experiment by adhering mixed-lipid membranes below their miscibility transition temperature. Thus, adhered membranes exhibited coexisting ordered and disordered phases in the free portion of the adhered vesicle as well as dark domains in the adhered portion of the same vesicle. We used the fluorescent dye Laurdan to resolve ordered and disordered phases simultaneously. Laurdan is excited *via* two-photon absorption at 780 nm but its emission spectrum depends upon the lipid phase; the peak emission wavelength for Laurdan in the

disordered phase is 490 nm but its peak emission in the ordered phase is 445nm. We treated the adhered vesicles with Laurdan and used two-photon microscopy to image them. We used the spectral shift properties to simultaneously image disordered and ordered phases by measuring I_{445} and I_{490}, the intensity of emitted light in two channels 445 nm and 490 nm respectively, and calculating $GP = (I_{445} - I_{490})/(I_{445} + I_{490})$. The GP measure confirmed the coexistence of ordered and disordered phases in the free portion of the vesicle but indicated there was no ordered phase present in the adhered portion of the vesicle even though the adhesion region exhibited dark domains.

Third, we used confocal reflection microscopy in conjunction with confocal fluorescence microscopy to image vesicles exhibiting dark domains in the adhesion region. The vesicle membrane had DiI incorporated and the binders had 488 nm dye conjugated to them. We confirmed that the dark domains excluded DiI and 488-avidin. However, we were unable to extract a reflection signal from the dark domain by reflecting light from it and this indicated the dark domain was not an intact membrane. If the dark domain were an intact membrane, we expected to successfully extract a reflection signal from the dark domain. In future experiments, this result could be sharpened by taking reflection images of an adhered vesicle using the 100X magnification objective to image confocal slices in 100 nm increments. Then a maximum intensity projection can be made, which is sensitive to contrast of index of refraction and not just to height differences.

Having demonstrated that the dark domains in adhered vesicles are holes, we turned to a second set of experiments. We switched from using ternary-mixture vesicles (DOPC:DPPC:CHOL) and used instead binary-mixture vesicles (DOPC:CHOL), which have been measured to be miscible at all experimentally relevant temperatures (10-50 °C) [76]. We adhered binary-mixture vesicles to solid supported membranes *via* biotin-avidin binding and found similar results: dark domains were formed in the adhesion zone. There was a major difference, however, in that the domains formed as small ($\sim 1\mu$m) fingers that grew into a complex pattern on a time scale $\sim$ 10-100 s. When we attempted to study these fingers in adhered vesicles, we found that the free portion of the membrane confounded the pattern formation process. In particular, as a fingering pattern formed, a portion of it grew near the boundary of the adhered vesicle. If the finger grew too close and breached the boundary, tension that had built up in the free portion of the membrane was released and the whole fingering pattern

collapsed. To circumvent this problem, which we wanted to do so we could study the full time evolution of the fingering pattern, we developed a new experimental method. We stabilized the adhered portion of the vesicle inside a thin ring ($\sim 1\mu$m) of immobile protein binders and removed the free portion of the vesicle by forcing it to rupture. This left a circular portion of adhered membrane where fingers grew internal to the immobile peripheral boundary.

When we studied the fingering pattern with ~ 5 s temporal resolution, we found that fingers grew intermittently at the boundary of an already formed hole. Fingers would form at random locations along the interface between previously-formed fingers and the protein-bound membrane. Then individual fingers each grew to a characteristic size and stopped. This process was iterated in the experiment. This suggested the formation of a finger was a thermally activated event. Thus, we adapted the theoretical models others had applied to pore formation in tense, free-floating vesicles where the rate of pore formation could be attributed to an activation energy [171, 175] and the growth dynamics of an ultimately stable pore was explained by the relaxation of an tense elastic film [173]. Furthermore, we saw that both the rate of finger formation and the size at which fingers arrested diminished as protein density of the membrane-bound region increased. We modeled the finger formation process as a thermally activated event governed by a free energy function that is modified as the density increases. Defining the normalized density ρ of the protein-bound region relative to the final density, we found that the width of the fingers $\lambda = 0.27 \pm 1.0\rho\,\mu$m and the height of the thermal activation energy barrier $\mathcal{F}^* = 3.8\rho$ kT.

The experimental system we have developed, which exhibits the pattern-forming process we have characterized, is worth developing further. It is a novel experimental system because a complex pattern that is formed inside the adhesion zone of lipid membranes bound with proteins exhibits time and length scales similar to those found in real cells. In the T-cell, for example, adhesion proteins and signaling molecules are dynamically arranged in micron-scale structures over the course of 5 to 10 minutes [154]. Moreover, when our fingering pattern is treated as a thermally activated process, the energy involved, a few kT, is on a biologically relevant scale. As far as we know, there are no other experimental examples that obtain all these features. Developing the system further would require learning more about it.

Two puzzles exist and may be related. First, if a growing finger arrests because the elastic stress in the membrane has been released, then that stress must by rein-

stated by some means so that another finger can form to again relax the membrane. The second puzzle concerns mass conservation; since the membrane that undergoes fingering is bound inside a circular frame and the fingers, which are holes, invade the protein bound region, the area spanned by protein-bound membrane decreases by 50% or more. It is impossible for a membrane to compress by that much—rupture strains in membranes are only about 1%—therefore the lipids must be leaving the bound membrane. If lipids are leaving the membrane, that would tend to increase the tension in the membrane (again because the outer frame is fixed).

There are two possible ways for the lipids to leave the membrane: one way is for lipids to be transferred into the free solution [173] and another way is for lipids to be transferred to the solid supported membrane [176]. The former possibility could be probed by varying the amount of cholesterol incorporated in the vesicle membrane that is adhered to the solid-supported membrane. DOPC:CHOL membranes cannot stably contain more than 70% cholesterol without expelling it from the membrane [76]. Therefore, increasing the faction of cholesterol would tend to increase the rate at which cholesterol is expelled from the membrane, which would tend to accelerate the finger-forming process. The latter possibility could be probed by adjusting the lipid composition of the solid-supported membrane. Currently the solid supported membrane contains ∼97% DOPC but incorporating large fractions of DPPC ($\sim 20\%$) would increase the chemical potential for cholesterol in the supported membrane. Thus, the rate at which tension was generated in the membrane would increase. Also, if lipids were transferred to the bottom layer so too should the DiI incorporated into the membrane bound protein. It may be possible to monitor the transfer of dye with fluorescence microscopy.

We expect that developing our experimental system further will allow us to study the pattern-forming dynamics with better precision. We also expect that sharpening the theoretical framework we use will allow us to link the dynamics in our system more closely to related systems including living cells. These are our tasks for the future.

Bibliography

[1] Vernita D Gordon, TJ O'Halloran, and O Shindell. Membrane adhesion and the formation of heterogeneities: biology, biophysics, and biotechnology. *Physical Chemistry Chemical Physics*, 17(24):15522–15533, 2015. 1, 10, 13, 19, 21

[2] O Shindell, N Mica, M Ritzer, and Vernita D Gordon. Specific adhesion of membranes simultaneously supports dual heterogeneities in lipids and proteins. *Physical Chemistry Chemical Physics*, 17(24):15598–15607, 2015. 1, 16, 29, 32, 34, 36, 37, 38, 40, 42, 43

[3] Patrick Lajoie, Jacky G Goetz, James W Dennis, and Ivan R Nabi. Lattices, rafts, and scaffolds: domain regulation of receptor signaling at the plasma membrane. *The Journal of cell biology*, 185(3):381–385, 2009. 5

[4] Antonella Viola and Neetu Gupta. Tether and trap: regulation of membrane-raft dynamics by actin-binding proteins. *Nature Reviews Immunology*, 7(11):889–896, 2007. 5

[5] Nagaraj Balasubramanian, David W Scott, J David Castle, James E Casanova, and Martin Alexander Schwartz. Arf6 and microtubules in adhesion-dependent trafficking of lipid rafts. *Nature cell biology*, 9(12):1381–1391, 2007. 5

[6] Michael P Sheetz, Julia E Sable, and Hans-Günther Döbereiner. Continuous membrane-cytoskeleton adhesion requires continuous accommodation to lipid and cytoskeleton dynamics. *Annu. Rev. Biophys. Biomol. Struct.*, 35:417–434, 2006. 5

[7] Santos Mañes and Antonella Viola. Lipid rafts in lymphocyte activation and migration (review). *Molecular membrane biology*, 23(1):59–69, 2006. 5

[8] Yan Yu, Nicole C Fay, Alexander A Smoligovets, Hung-Jen Wu, and Jay T Groves. Myosin iia modulates t cell receptor transport and casl phosphorylation during early immunological synapse formation. *PloS one*, 7(2):e30704, 2012. 5

[9] Pradeep M Nair, Khalid Salaita, Rebecca S Petit, and Jay T Groves. Using patterned supported lipid membranes to investigate the role of receptor organization in intercellular signaling. *Nature protocols*, 6(4):523–539, 2011. 5, 26, 27

[10] Kai Simons and Elina Ikonen. Functional rafts in cell membranes. *Nature*, 387(6633):569, 1997. 5, 23

[11] K Simons and E Ikonen. Sphingolipid-cholesterol rafts in membrane trafficking and signalling. *Nature*, 387:569–572, 1997. 5

[12] Daniel Lingwood and Kai Simons. Lipid rafts as a membrane-organizing principle. *science*, 327(5961):46–50, 2010. 5, 23

[13] Michael Edidin. The state of lipid rafts: from model membranes to cells. *Annual review of biophysics and biomolecular structure*, 32(1):257–283, 2003. 5, 23

[14] Kai Simons and Winchil LC Vaz. Model systems, lipid rafts, and cell membranes 1. *Annu. Rev. Biophys. Biomol. Struct.*, 33:269–295, 2004. 5, 23

[15] Linda J Pike. Rafts defined: a report on the keystone symposium on lipid rafts and cell function. *Journal of lipid research*, 47(7):1597–1598, 2006. 5, 23

[16] Donald M Engelman. Membranes are more mosaic than fluid. *Nature*, 438(7068):578–580, 2005. 5

[17] Boryana N Manz, Bryan L Jackson, Rebecca S Petit, Michael L Dustin, and Jay Groves. T-cell triggering thresholds are modulated by the number of antigen within individual t-cell receptor clusters. *Proceedings of the National Academy of Sciences*, 108(22):9089–9094, 2011. 5

[18] Jay T Groves. Molecular organization and signal transduction at intermembrane junctions. *Angewandte Chemie International Edition*, 44(23):3524–3538, 2005. 5

[19] Ilya Levental, Michal Grzybek, and Kai Simons. Raft domains of variable properties and compositions in plasma membrane vesicles. *Proceedings of the National Academy of Sciences*, 108(28):11411–11416, 2011. 5

[20] Tobias Baumgart, Adam T Hammond, Prabuddha Sengupta, Samuel T Hess, David A Holowka, Barbara A Baird, and Watt W Webb. Large-scale fluid/fluid phase separation of proteins and lipids in giant plasma membrane vesicles. *Proceedings of the National Academy of Sciences*, 104(9):3165–3170, 2007. 5

[21] Sarah L Veatch, Pietro Cicuta, Prabuddha Sengupta, Aurelia Honerkamp-Smith, David Holowka, and Barbara Baird. Critical fluctuations in plasma membrane vesicles. *ACS chemical biology*, 3(5):287–293, 2008. 5, 14

[22] Aurelia R Honerkamp-Smith, Sarah L Veatch, and Sarah L Keller. An introduction to critical points for biophysicists; observations of compositional heterogeneity in lipid membranes. *Biochimica et Biophysica Acta (BBA)-Biomembranes*, 1788(1):53–63, 2009. 5

[23] Daniel Lingwood, Jonas Ries, Petra Schwille, and Kai Simons. Plasma membranes are poised for activation of raft phase coalescence at physiological temperature. *Proceedings of the National Academy of Sciences*, 105(29):10005–10010, 2008. 5

[24] Artem G Ayuyan and Fredric S Cohen. Raft composition at physiological temperature and ph in the absence of detergents. *Biophysical journal*, 94(7):2654–2666, 2008. 5

[25] Pranav Sharma, Rajat Varma, RC Sarasij, Karine Gousset, G Krishnamoorthy, Madan Rao, Satyajit Mayor, et al. Nanoscale organization of multiple gpi-anchored proteins in living cell membranes. *Cell*, 116(4):577–589, 2004. 5

[26] Joanna C Porter and Nancy Hogg. Integrins take partners: cross-talk between integrins and other membrane receptors. *Trends in cell biology*, 8(10):390–396, 1998. 5

[27] Laurence Decker et al. Lipid rafts and integrin activation regulate oligodendrocyte survival. *Journal of Neuroscience*, 24(15):3816–3825, 2004. 5

[28] Christine Salaün, Gwyn W Gould, and Luke H Chamberlain. Lipid raft association of snare proteins regulates exocytosis in pc12 cells. *Journal of Biological Chemistry*, 280(20):19449–19453, 2005. 5

[29] Luke H Chamberlain, Robert D Burgoyne, and Gwyn W Gould. Snare proteins are highly enriched in lipid rafts in pc12 cells: implications for the spatial control of exocytosis. *Proceedings of the National Academy of Sciences*, 98(10):5619–5624, 2001. 5

[30] Niti Puri and Paul A Roche. Ternary snare complexes are enriched in lipid rafts during mast cell exocytosis. *Traffic*, 7(11):1482–1494, 2006. 5

[31] Meritxell Reverter, Carles Rentero, Sandra Vilà de Muga, Anna Alvarez-Guaita, Vishwaroop Mulay, Rose Cairns, Peta Wood, Katia Monastyrskaya, Albert Pol, Francesc Tebar, et al. Cholesterol transport from late endosomes to the golgi regulates t-snare trafficking, assembly, and function. *Molecular biology of the cell*, 22(21):4108–4123, 2011. 5

[32] Michael L Dustin and Jay T Groves. Receptor signaling clusters in the immune synapse. *Annual review of biophysics*, 41:543–556, 2012. 6

[33] Michael L Dustin, Arup K Chakraborty, and Andrey S Shaw. Understanding the structure and function of the immunological synapse. *Cold Spring Harbor perspectives in biology*, 2(10):a002311, 2010. 6

[34] Tamas Fulop, Aurélie Le Page, Hugo Garneau, Naheed Azimi, Sarra Baehl, Gilles Dupuis, Graham Pawelec, and Anis Larbi. Aging, immunosenescence and membrane rafts: the lipid connection. *Longevity & Healthspan*, 1(1):6, 2012. 6

[35] Oliver Purrucker, Stefanie Gönnenwein, Anton Förtig, Rainer Jordan, Monika Rusp, Michael Bärmann, Luis Moroder, Erich Sackmann, and Motomu Tanaka. Polymer-tethered membranes as quantitative models for the study of integrin-mediated cell adhesion. *Soft Matter*, 3(3):333–336, 2007. 7, 19

[36] Ana-Sunčana Smith, Kheya Sengupta, Stefanie Goennenwein, Udo Seifert, and Erich Sackmann. Force-induced growth of adhesion domains is controlled by receptor mobility. *Proceedings of the National Academy of Sciences*, 105(19):6906–6911, 2008. 7, 19

[37] Minsub Chung, Randall D Lowe, Yee-Hung M Chan, Prasad V Ganesan, and Steven G Boxer. Dna-tethered membranes formed by giant vesicle rupture. *Journal of structural biology*, 168(1):190–199, 2009. 7, 19

[38] Bettina van Lengerich, Robert J Rawle, and Steven G Boxer. Covalent attachment of lipid vesicles to a fluid-supported bilayer allows observation of dna-mediated vesicle interactions. *Langmuir*, 26(11):8666–8672, 2010. 7, 19

[39] Tomas D Perez, W James Nelson, Steven G Boxer, and Lance Kam. E-cadherin tethered to micropatterned supported lipid bilayers as a model for cell adhesion. *Langmuir*, 21(25):11963–11968, 2005. 7, 19

[40] Susanne Franziska Fenz, Ana-Sunčana Smith, Rudolf Merkel, and Kheya Sengupta. Inter-membrane adhesion mediated by mobile linkers: effect of receptor shortage. *Soft Matter*, 7(3):952–962, 2011. 7, 8, 24, 31, 45, 62

[41] Ana-Sunčana Smith and Erich Sackmann. Progress in mimetic studies of cell adhesion and the mechanosensing. *ChemPhysChem*, 10(1):66–78, 2009. 7, 8

[42] Ellen Reister-Gottfried, Kheya Sengupta, Barbara Lorz, Erich Sackmann, Udo Seifert, and Ana-Sunčana Smith. Dynamics of specific vesicle-substrate adhesion: from local events to global dynamics. *Physical review letters*, 101(20):208103, 2008. 7, 8, 11, 62

[43] Cornelia Monzel, Susanne F Fenz, Rudolf Merkel, and Kheya Sengupta. Probing biomembrane dynamics by dual-wavelength reflection interference contrast microscopy. *ChemPhysChem*, 10(16):2828–2838, 2009. 7, 8

[44] Laurent Limozin and Kheya Sengupta. Quantitative reflection interference contrast microscopy (ricm) in soft matter and cell adhesion. *ChemPhysChem*, 10(16):2752–2768, 2009. 7, 8

[45] Damien Cuvelier and Pierre Nassoy. Hidden dynamics of vesicle adhesion induced by specific stickers. *Physical review letters*, 93(22):228101, 2004. 7, 8

[46] P-H Puech, V Askovic, P-G De Gennes, and F Brochard-Wyart. Dynamics of vesicle adhesion: spreading versus dewetting coupled to binder diffusion. *Biophysical Reviews and Letters*, 1(01):85–95, 2006. 7, 8, 11

[47] P-H Puech, H Feracci, and F Brochard-Wyart. Adhesion between giant vesicles and supported bilayers decorated with chelated e-cadherin fragments. *Langmuir*, 20(22):9763–9768, 2004. 7, 8

[48] Erich Sackmann and Robijn F Bruinsma. Cell adhesion as wetting transition? *ChemPhysChem*, 3(3):262–269, 2002. 7, 8, 62

[49] Susanne F Fenz, Timo Bihr, Rudolf Merkel, Udo Seifert, Kheya Sengupta, and Ana-Sunčana Smith. Switching from ultraweak to strong adhesion. *Advanced materials*, 23(22-23):2622–2626, 2011. 7, 8

[50] Heinrich Krobath, Bartosz Różycki, Reinhard Lipowsky, and Thomas R Weikl. Line tension and stability of domains in cell-adhesion zones mediated by long and short receptor-ligand complexes. *PLoS One*, 6(8):e23284, 2011. 7, 8

[51] TR Weikl, JT Groves, and R Lipowsky. Pattern formation during adhesion of multicomponent membranes. *EPL (Europhysics Letters)*, 59(6):916, 2002. 7, 8

[52] Thomas R Weikl, Mesfin Asfaw, Heinrich Krobath, Bartosz Różycki, and Reinhard Lipowsky. Adhesion of membranes via receptor–ligand complexes: Domain formation, binding cooperativity, and active processes. *Soft Matter*, 5(17):3213–3224, 2009. 7, 8

[53] HGJS Krobath, GJ Schütz, R Lipowsky, and TR Weikl. Lateral diffusion of receptor-ligand bonds in membrane adhesion zones: Effect of thermal membrane roughness. *EPL (Europhysics Letters)*, 78(3):38003, 2007. 7, 8

[54] B Różycki, Reinhard Lipowsky, and Thomas R Weikl. Segregation of receptor–ligand complexes in cell adhesion zones: phase diagrams and the role of thermal membrane roughness. *New Journal of Physics*, 12(9):095003, 2010. 7, 8, 30

[55] Heinrich Krobath, Bartosz Różycki, Reinhard Lipowsky, and Thomas R Weikl. Binding cooperativity of membrane adhesion receptors. *Soft Matter*, 5(17):3354–3361, 2009. 7, 8

[56] Joachim Rädler and Erich Sackmann. Imaging optical thicknesses and separation distances of phospholipid vesicles at solid surfaces. *Journal de Physique II*, 3(5):727–748, 1993. 7, 8

[57] Susanne F Fenz, Rudolf Merkel, and Kheya Sengupta. Diffusion and intermembrane distance: case study of avidin and e-cadherin mediated adhesion. *Langmuir*, 25(2):1074–1085, 2008. 7, 24

[58] Daniel Axelrod. Cell-substrate contacts illuminated by total internal reflection fluorescence. *The Journal of cell biology*, 89(1):141–145, 1981. 8

[59] Jay T Groves, Raghuveer Parthasarathy, and Martin B Forstner. Fluorescence imaging of membrane dynamics. *Annu. Rev. Biomed. Eng.*, 10:311–338, 2008. 8

[60] A Albersdörfer, T Feder, and E Sackmann. Adhesion-induced domain formation by interplay of long-range repulsion and short-range attraction force: a model membrane study. *Biophysical journal*, 73(1):245–257, 1997. 8, 24, 62

[61] Alexei Boulbitch, Zeno Guttenberg, and Erich Sackmann. Kinetics of membrane adhesion mediated by ligand–receptor interaction studied with a biomimetic system. *Biophysical Journal*, 81(5):2743–2751, 2001. 8, 11, 24, 62

[62] Annette Kloboucek, Almuth Behrisch, Jan Faix, and Erich Sackmann. Adhesion-induced receptor segregation and adhesion plaque formation: a model membrane study. *Biophysical journal*, 77(4):2311–2328, 1999. 8, 24, 62

[63] Motomu Tanaka and Erich Sackmann. Polymer-supported membranes as models of the cell surface. *Nature*, 437(7059):656–663, 2005. 8

[64] Ana-Sunčana Smith, Barbara G Lorz, Udo Seifert, and Erich Sackmann. Antagonist-induced deadhesion of specifically adhered vesicles. *Biophysical journal*, 90(3):1064–1080, 2006. 8

[65] E Evans and W Rawicz. Entropy-driven tension and bending elasticity in condensed-fluid membranes. *Physical Review Letters*, 64(17):2094, 1990. 13, 15

[66] Erdinc Sezgin, Hermann-Josef Kaiser, Tobias Baumgart, Petra Schwille, Kai Simons, and Ilya Levental. Elucidating membrane structure and protein behavior using giant plasma membrane vesicles. *nature protocols*, 7(6):1042–1051, 2012. 14

[67] Ruby May A Sullan, James K Li, Changchun Hao, Gilbert C Walker, and Shan Zou. Cholesterol-dependent nanomechanical stability of phase-segregated multicomponent lipid bilayers. *Biophysical journal*, 99(2):507–516, 2010. 14

[68] Hermann-Josef Kaiser, Daniel Lingwood, Ilya Levental, Julio L Sampaio, Lucie Kalvodova, Lawrence Rajendran, and Kai Simons. Order of lipid phases in model and plasma membranes. *Proceedings of the National Academy of Sciences*, 106(39):16645–16650, 2009. 14

[69] Ilya Levental, Fitzroy J Byfield, Pramit Chowdhury, Feng Gai, Tobias Baumgart, and Paul A Janmey. Cholesterol-dependent phase separation in cell-derived giant plasma-membrane vesicles. *Biochemical Journal*, 424(2):163–167, 2009. 14

[70] Sarah L Veatch. From small fluctuations to large-scale phase separation: lateral organization in model membranes containing cholesterol. In *Seminars in cell & developmental biology*, volume 18, pages 573–582. Elsevier, 2007. 14

[71] Gerald W Feigenson. Phase boundaries and biological membranes. *Annu. Rev. Biophys. Biomol. Struct.*, 36:63–77, 2007. 14

[72] Sarah L Veatch and Sarah L Keller. Miscibility phase diagrams of giant vesicles containing sphingomyelin. *Physical review letters*, 94(14):148101, 2005. 14

[73] Mary Elizabeth Beattie, Sarah L Veatch, Benjamin L Stottrup, and Sarah L Keller. Sterol structure determines miscibility versus melting transitions in lipid vesicles. *Biophysical journal*, 89(3):1760–1768, 2005. 14

[74] Harden M McConnell and Marija Vrljic. Liquid-liquid immiscibility in membranes. *Annual review of biophysics and biomolecular structure*, 32(1):469–492, 2003. 14

[75] Sarah L Veatch and Sarah L Keller. Organization in lipid membranes containing cholesterol. *Physical Review Letters*, 89(26):268101, 2002. 14, 24, 35, 62

[76] Sarah L Veatch and Sarah L Keller. Separation of liquid phases in giant vesicles of ternary mixtures of phospholipids and cholesterol. *Biophysical journal*, 85(5):3074–3083, 2003. 14, 24, 28, 33, 44, 54, 55, 62, 64, 66

[77] Suliana Manley and Vernita D Gordon. Making giant unilamellar vesicles via hydration of a lipid film. *Current protocols in cell biology*, pages 24–3, 2008. 14

[78] VD Gordon, PA Beales, Z Zhao, C Blake, FC MacKintosh, PD Olmsted, ME Cates, SU Egelhaaf, and WCK Poon. Lipid organization and the morphology of solid-like domains in phase-separating binary lipid membranes. *Journal of Physics: Condensed Matter*, 18(32):L415, 2006. 14, 39, 45

[79] Sarah L Veatch, Klaus Gawrisch, and Sarah L Keller. Closed-loop miscibility gap and quantitative tie-lines in ternary membranes containing diphytanoyl pc. *Biophysical journal*, 90(12):4428–4436, 2006. 14, 24, 33, 41, 43

[80] Cynthia A Stanich, Aurelia R Honerkamp-Smith, Gregory Garbes Putzel, Christopher S Warth, Andrea K Lamprecht, Pritam Mandal, Elizabeth Mann, Thien-An D Hua, and Sarah L Keller. Coarsening dynamics of domains in lipid membranes. *Biophysical journal*, 105(2):444–454, 2013. 15, 62

[81] Wolfgang Helfrich. Elastic properties of lipid bilayers: theory and possible experiments. *Zeitschrift für Naturforschung C*, 28(11-12):693–703, 1973. 15

[82] F Brochard, PG De Gennes, and P Pfeuty. Surface tension and deformations of membrane structures: relation to two-dimensional phase transitions. *Journal de Physique*, 37(10):1099–1104, 1976. 15

[83] Thomas Portet, Sharona E Gordon, and Sarah L Keller. Increasing membrane tension decreases miscibility temperatures; an experimental demonstration via micropipette aspiration. *Biophysical journal*, 103(8):L35–L37, 2012. 15, 24

[84] Tsutomu Hamada, Yuko Kishimoto, Takeshi Nagasaki, and Masahiro Takagi. Lateral phase separation in tense membranes. *Soft Matter*, 7(19):9061–9068, 2011. 15, 24, 44

[85] Vernita D Gordon, Markus Deserno, CMJ Andrew, SU Egelhaaf, and WCK Poon. Adhesion promotes phase separation in mixed-lipid membranes. *EPL (Europhysics Letters)*, 84(4):48003, 2008. 15, 16, 24, 30, 31, 62

[86] Mark J Uline, M Schick, and Igal Szleifer. Phase behavior of lipid bilayers under tension. *Biophysical journal*, 102(3):517–522, 2012. 16

[87] Raghuveer Parthasarathy, Cheng-han Yu, and Jay T Groves. Curvature-modulated phase separation in lipid bilayer membranes. *Langmuir*, 22(11):5095–5099, 2006. 16, 24, 30

[88] Paul A Beales, Jin Nam, and T Kyle Vanderlick. Specific adhesion between dna-functionalized ?janus? vesicles: size-limited clusters. *Soft Matter*, 7(5):1747–1755, 2011. 16

[89] Jiang Zhao, Jing Wu, and SarahL. Veatch. Adhesion stabilizes robust lipid heterogeneity in supercritical membranes at physiological temperature. *Biophysical Journal*, 104(4):825 – 834, 2013. 16, 40, 41

[90] Yanxiang Zhao, Sovan Das, and Qiang Du. Adhesion of multicomponent vesicle membranes. *Physical Review E*, 81(4):041919, 2010. 17, 24, 30

[91] Tahereh Rouhiparkouhi, Thomas R Weikl, Dennis E Discher, and Reinhard Lipowsky. Adhesion-induced phase behavior of two-component membranes and vesicles. *International journal of molecular sciences*, 14(1):2203–2229, 2013. 17, 29

[92] Tianshun Lian and Rodney JY Ho. Trends and developments in liposome drug delivery systems. *Journal of pharmaceutical sciences*, 90(6):667–680, 2001. 17

[93] Jaymin C Shah, Yogesh Sadhale, and Dakshina Murthy Chilukuri. Cubic phase gels as drug delivery systems. *Advanced drug delivery reviews*, 47(2):229–250, 2001. 17

[94] Robert Langer. Drug delivery abd targeting. *Nature*, 392(6679):5–10, 1998. 17

[95] Gregor Cevc. Lipid vesicles and other colloids as drug carriers on the skin. *Advanced drug delivery reviews*, 56(5):675–711, 2004. 17

[96] Shao-Ling Huang and Robert C MacDonald. Acoustically active liposomes for drug encapsulation and ultrasound-triggered release. *Biochimica et Biophysica Acta (BBA)-Biomembranes*, 1665(1):134–141, 2004. 17

[97] Dennis E Discher and Adi Eisenberg. Polymer vesicles. *Science*, 297(5583):967–973, 2002. 17

[98] Gopal R Anyarambhatla and David Needham. Enhancement of the phase transition permeability of dppc liposomes by incorporation of mppc: a new temperature-sensitive liposome for use with mild hyperthermia. *Journal of liposome research*, 9(4):491–506, 1999. 17

[99] Emma Sparr, Christoffer Åberg, Peter Nilsson, and Håkan Wennerström. Diffusional transport in responding lipid membranes. *Soft Matter*, 5(17):3225–3233, 2009. 17

[100] AG Lee. Lipid phase transitions and phase diagrams i. lipid phase transitions. *Biochimica et Biophysica Acta (BBA)-Reviews on Biomembranes*, 472(2):237–281, 1977. 17

[101] D Papahadjopoulos, K Jacobson, S Nir, and I Isac. Phase transitions in phospholipid vesicles fluorescence polarization and permeability measurements concerning the effect of temperature and cholesterol. *Biochimica et Biophysica Acta (BBA)-Biomembranes*, 311(3):330–348, 1973. 17

[102] MC Blok, ECM Van der Neut-Kok, LLM Van Deenen, and J De Gier. The effect of chain length and lipid phase transitions on the selective permeability properties of liposomes. *Biochimica et Biophysica Acta (BBA)-Biomembranes*, 406(2):187–196, 1975. 17

[103] Jens Risbo, Kent Jørgensen, Maria M Sperotto, and Ole G Mouritsen. Phase behavior and permeability properties of phospholipid bilayers containing a short-chain phospholipid permeability enhancer. *Biochimica et Biophysica Acta (BBA)-Biomembranes*, 1329(1):85–96, 1997. 17

[104] G Kong and MW Dewhirst. Review hyperthermia and liposomes. *International Journal of Hyperthermia*, 15(5):345–370, 1999. 17

[105] Milton B Yatvin, John N Weinstein, Warren H Dennis, and Robert Blumenthal. Design of liposomes for enhanced local release of drugs by hyperthermia. *Science*, 202(4374):1290–1293, 1978. 18

[106] Anu Puri, Kristin Loomis, Brandon Smith, Jae-Ho Lee, Amichai Yavlovich, Eliahu Heldman, and Robert Blumenthal. Lipid-based nanoparticles as pharma-

ceutical drug carriers: from concepts to clinic. *Critical Reviews? in Therapeutic Drug Carrier Systems*, 26(6), 2009. 18

[107] Christoph Mamot, Daryl C Drummond, Udo Greiser, Keelung Hong, Dmitri B Kirpotin, James D Marks, and John W Park. Epidermal growth factor receptor (egfr)-targeted immunoliposomes mediate specific and efficient drug delivery to egfr-and egfrviii-overexpressing tumor cells. *Cancer research*, 63(12):3154–3161, 2003. 19

[108] Erika Bohl Kullberg, Nill Bergstrand, Jörgen Carlsson, Katarina Edwards, Markus Johnsson, Stefan Sjöberg, and Lars Gedda. Development of egf-conjugated liposomes for targeted delivery of boronated dna-binding agents. *Bioconjugate chemistry*, 13(4):737–743, 2002. 19

[109] Ernst Wagner, David Curiel, and Matt Cotten. Delivery of drugs, proteins and genes into cells using transferrin as a ligand for receptor-mediated endocytosis. *Advanced Drug Delivery Reviews*, 14(1):113–135, 1994. 19

[110] Zhong Ming Qian, Hongyan Li, Hongzhe Sun, and Kwokping Ho. Targeted drug delivery via the transferrin receptor-mediated endocytosis pathway. *Pharmacological reviews*, 54(4):561–587, 2002. 19

[111] Tomoyuki Kakudo, Shinji Chaki, Shiroh Futaki, Ikuhiko Nakase, Kenichi Akaji, Toru Kawakami, Kazuo Maruyama, Hiroyuki Kamiya, and Hideyoshi Harashima. Transferrin-modified liposomes equipped with a ph-sensitive fusogenic peptide: an artificial viral-like delivery system. *Biochemistry*, 43(19):5618–5628, 2004. 19

[112] MMGMRPARGADJCMC Colin, M Maurice, G Trugnan, M Kornprobst, RP Harbottle, A Knight, RG Cooper, AD Miller, J Capeau, C Coutelle, et al. Cell delivery, intracellular trafficking and expression of an integrin-mediated gene transfer vector in tracheal epithelial cells. *Gene therapy*, 7(2):139, 2000. 19

[113] Cheng-han Yu and Jay T Groves. Engineering supported membranes for cell biology. *Medical & biological engineering & computing*, 48(10):955–963, 2010. 19

[114] Conlin P O'Neil, André J van der Vlies, Diana Velluto, Christine Wandrey, Davide Demurtas, Jacques Dubochet, and Jeffrey A Hubbell. Extracellular matrix binding mixed micelles for drug delivery applications. *Journal of Controlled Release*, 137(2):146–151, 2009. 19

[115] Jeffrey A Hubbell and Dominique A Rothenfluh. Polypeptide ligands for targeting cartilage and methods of use thereof, September 22 2009. US Patent 7,592,009. 19

[116] Julie C Liu and David A Tirrell. Cell response to rgd density in cross-linked artificial extracellular matrix protein films. *Biomacromolecules*, 9(11):2984–2988, 2008. 19

[117] Qingtao Liu and Ben J Boyd. Liposomes in biosensors. *Analyst*, 138(2):391–409, 2013. 20

[118] Hsiao-Wei Wen, Wlodzimierz Borejsza-Wysocki, Thomas R DeCory, and Richard A Durst. Development of a competitive liposome-based lateral flow assay for the rapid detection of the allergenic peanut protein ara h1. *Analytical and bioanalytical chemistry*, 382(5):1217–1226, 2005. 20

[119] Hsiao-Wei Wen, Wlodzimierz Borejsza-Wysocki, Thomas R DeCory, Antje J Baeumner, and Richard A Durst. A novel extraction method for peanut allergenic proteins in chocolate and their detection by a liposome-based lateral flow assay. *European Food Research and Technology*, 221(3-4):564–569, 2005. 20

[120] Stuart G Reeves, Sui Ti A Siebert, Matthew A Roberts, and Richard A Durst. Liposome immunosensing devices for environmental contaminant screening. *TrAC Trends in Analytical Chemistry*, 14(7):351–355, 1995. 20

[121] Soohyoun Ahn-Yoon, Thomas R DeCory, and Richard A Durst. Ganglioside–liposome immunoassay for the detection of botulinum toxin. *Analytical and bioanalytical chemistry*, 378(1):68–75, 2004. 20

[122] Soohyoun Ahn and Richard A Durst. Detection of cholera toxin in seafood using a ganglioside-liposome immunoassay. *Analytical and bioanalytical chemistry*, 391(2):473–478, 2008. 20

[123] Sungsu Park and Richard A Durst. Immunoliposome sandwich assay for the detection of escherichia coli o157: H7. *Analytical biochemistry*, 280(1):151–158, 2000. 20

[124] Shruti Shukla, Jaehyuk Bang, Seunggi Heu, and Myunghee Kim. Development of immunoliposome-based assay for the detection of salmonella typhimurium. *European Food Research and Technology*, 234(1):53–59, 2012. 20

[125] Myunghee KIM, Sejong OH, and Richard A Durst. Detection of escherichia coli o157: H7 using combined procedure of immunomagnetic separation and test strip liposome immunoassay. *Journal of microbiology and biotechnology*, 13(4):509–516, 2003. 20

[126] Ja-an Annie Ho, Shi-Chin Zeng, Wei-Hsiang Tseng, Yong-Jen Lin, and Chun-hsien Chen. Liposome-based immunostrip for the rapid detection of salmonella. *Analytical and bioanalytical chemistry*, 391(2):479–485, 2008. 20

[127] Ja-an Annie Ho and Hsiu-Wen Hsu. Procedures for preparing escherichia c oli o157: H7 immunoliposome and its application in liposome immunoassay. *Analytical chemistry*, 75(16):4330–4334, 2003. 20

[128] Antje J Baeumner, Barbara Leonard, John McElwee, and Richard A Montagna. A rapid biosensor for viable b. anthracis spores. *Analytical and bioanalytical chemistry*, 380(1):15–23, 2004. 20

[129] Harriet A Hartley and Antje J Baeumner. Biosensor for the specific detection of a single viable b. áanthracis spore. *Analytical and bioanalytical chemistry*, 376(3):319–327, 2003. 20

[130] Antje J Baeumner, Nicole A Schlesinger, Naomi S Slutzki, Joseph Romano, Eun Mi Lee, and Richard A Montagna. Biosensor for dengue virus detection: sensitive, rapid, and serotype specific. *Analytical chemistry*, 74(6):1442–1448, 2002. 20

[131] Vijayarani Kumanan, Sam R Nugen, Antje J Baeumner, and Yung-Fu Chang. A biosensor assay for the detection of mycobacterium avium subsp. paratuberculosis in fecal samples. *Journal of veterinary science*, 10(1):35–42, 2009. 20

[132] Mieko Horie, Hiroyuki Yanagisawa, and Masao Sugawara. Fluorometric immunoassay based on ph-sensitive dye-encapsulating liposomes and gramicidin channels. *Analytical biochemistry*, 369(2):192–201, 2007. 20

[133] Jayati Banerjee, Andrea J Hanson, Erin K Nyren-Erickson, Bratati Ganguli, Anil Wagh, Wallace W Muhonen, Benedict Law, John B Shabb, DK Srivastava, and Sanku Mallik. Liposome-mediated amplified detection of cell-secreted matrix metalloproteinase-9. *Chemical Communications*, 46(18):3209–3211, 2010. 20

[134] HAH Rongen, HM Van der Horst, GWK Hugenholtz, A Bult, WP Van Bennekom, and PH Van der Meide. Development of a liposome immunosorbent assay for human interferon-y. *Analytica chimica acta*, 287(3):191–199, 1994. 20

[135] HAH Rongen, T Van Nierop, HM Van der Horst, RFM Rombouts, PH Van der Meide, A Bult, and WP Van Bennekom. Biotinylated and streptavidinylated liposomes as labels in cytokine immunoassays. *Analytica chimica acta*, 306(2-3):333–341, 1995. 20

[136] Katie A Edwards and John C March. Gm 1-functionalized liposomes in a microtiter plate assay for cholera toxin in vibrio cholerae culture samples. *Analytical biochemistry*, 368(1):39–48, 2007. 20

[137] Ja-an Annie Ho, Li-Chen Wu, Ming-Ray Huang, Yong-Jen Lin, Antje J Baeumner, and Richard A Durst. Application of ganglioside-sensitized liposomes in a flow injection immunoanalytical system for the determination of cholera toxin. *Analytical chemistry*, 79(1):246–250, 2007. 20

[138] Ja-an Annie Ho, Hsiu-Wen Hsu, and Ming-Ray Huang. Liposome-based microcapillary immunosensor for detection of escherichia coli o157: H7. *Analytical biochemistry*, 330(2):342–349, 2004. 20

[139] Subramanian Viswanathan, Li-chen Wu, Ming-Ray Huang, and Ja-an Annie Ho. Electrochemical immunosensor for cholera toxin using liposomes and poly (3, 4-ethylenedioxythiophene)-coated carbon nanotubes. *Analytical chemistry*, 78(4):1115–1121, 2006. 20

[140] Bo Qu, Lei Guo, Xia Chu, Dan-Hong Wu, Guo-Li Shen, and Ru-Qin Yu. An electrochemical immunosensor based on enzyme-encapsulated liposomes and biocatalytic metal deposition. *Analytica chimica acta*, 663(2):147–152, 2010. 20

[141] Naoyoshi Egashira, Shin-ichi Morita, Emi Hifumi, Yoshiharu Mitoma, and Taizo Uda. Attomole detection of hemagglutinin molecule of influenza virus by combining an electrochemiluminescence sensor with an immunoliposome that encapsulates a ru complex. *Analytical chemistry*, 80(11):4020–4025, 2008. 20

[142] Huan Chen, Yue Zheng, Jian-Hui Jiang, Hai-Long Wu, Guo-Li Shen, and Ru-Qin Yu. An ultrasensitive chemiluminescence biosensor for cholera toxin based on ganglioside-functionalized supported lipid membrane and liposome. *Biosensors and Bioelectronics*, 24(4):684–689, 2008. 20

[143] Yue Zheng, Huan Chen, Xue-Ping Liu, Jian-Hui Jiang, Yan Luo, Guo-Li Shen, and Ru-Qin Yu. An ultrasensitive chemiluminescence immunosensor for psa based on the enzyme encapsulated liposome. *Talanta*, 77(2):809–814, 2008. 20

[144] NT Thet, SH Hong, S Marshall, M Laabei, A Toby, and A Jenkins. Visible, colorimetric dissemination between pathogenic strains of staphylococcus aureus and pseudomonas aeruginosa using fluorescent dye containing lipid vesicles. *Biosensors and Bioelectronics*, 41:538–543, 2013. 20

[145] Gregor Cevc and Holger Richardsen. Lipid vesicles and membrane fusion. *Advanced Drug Delivery Reviews*, 38(3):207–232, 1999. 20

[146] Harma Ellens, Joe Bentz, and Francis C Szoka. ph-induced destabilization of phosphatidylethanolamine-containing liposomes: role of bilayer contact. *Biochemistry*, 23(7):1532–1538, 1984. 20

[147] Jerome Connor, Milton B Yatvin, and Leaf Huang. ph-sensitive liposomes: acid-induced liposome fusion. *Proceedings of the National Academy of Sciences*, 81(6):1715–1718, 1984. 20

[148] David Collins, David C Litzinger, and Leaf Huang. Structural and functional comparisons of ph-sensitive liposomes composed of phosphatidylethanolamine

and three different diacylsuccinylglycerols. *Biochimica et Biophysica Acta (BBA)-Biomembranes*, 1025(2):234–242, 1990. 20

[149] RJ Ho, BT Rouse, and L Huang. Target-sensitive immunoliposomes as an efficient drug carrier for antiviral activity. *Journal of Biological Chemistry*, 262(29):13973–13978, 1987. 20

[150] Purnima Pinnaduwage and Leaf Huang. Stable target-sensitive immunoliposomes. *Biochemistry*, 31(11):2850–2855, 1992. 20

[151] G Cevc. Agent targeting by means of the chemically or physically directed, fusogenic liposomes. *Journal of Liposome Research*, 6(4):643–663, 1996. 20

[152] John F Hancock. Lipid rafts: contentious only from simplistic standpoints. *Nature Reviews Molecular Cell Biology*, 7(6):456–462, 2006. 23

[153] Tobias Baumgart, Samuel T Hess, and Watt W Webb. Imaging coexisting fluid domains in biomembrane models coupling curvature and line tension. *Nature*, 425(6960):821–824, 2003. 24, 35

[154] Arash Grakoui, Shannon K Bromley, Cenk Sumen, Mark M Davis, Andrey S Shaw, Paul M Allen, and Michael L Dustin. The immunological synapse: a molecular machine controlling t cell activation. *Science*, 285(5425):221–227, 1999. 24, 47, 49, 65

[155] Shannon K Bromley, W Richard Burack, Kenneth G Johnson, Kristina Somersalo, Tasha N Sims, Cenk Sumen, Mark M Davis, Andrey S Shaw, Paul M Allen, and Michael L Dustin. The immunological synapse. *Annual review of immunology*, 19(1):375–396, 2001. 24, 47

[156] Hae Won Sohn, Pavel Tolar, and Susan K Pierce. Membrane heterogeneities in the formation of b cell receptor–lyn kinase microclusters and the immune synapse. *The Journal of cell biology*, 182(2):367–379, 2008. 24, 47

[157] Michael L Dustin and John A Cooper. The immunological synapse and the actin cytoskeleton: molecular hardware for t cell signaling. *Nature immunology*, 1(1):23–29, 2000. 24, 47

[158] SY Qi, Jay T Groves, and Arup K Chakraborty. Synaptic pattern formation during cellular recognition. *Proceedings of the National Academy of Sciences*, 98(12):6548–6553, 2001. 24, 47, 49

[159] Alexander I Norman, Brittney A Manvilla, Evan L Frank, Justine N Niamke, Grant D Smith, and Sandra C Greer. Partitioning of poly (ethylene oxide), poly (ethylene imide), and bovine serum albumin in isobutyric acid+ water. *Macromolecules*, 41(3):997–1008, 2008. 25

[160] Miglena I Angelova and Dimiter S Dimitrov. Liposome electroformation. *Faraday discussions of the Chemical Society*, 81:303–311, 1986. 25

[161] Matthew I Hoopes, Roland Faller, and Marjorie L Longo. Lipid domain depletion at small localized bends imposed by a step geometry. *Langmuir*, 27(6):2783–2788, 2011. 30

[162] Herbert B Callen. Thermodynamics and an introduction to thermostatistics, 1998. 35

[163] Marilyn B Schneider, WINSTON K Chan, and Watt W Webb. Fast diffusion along defects and corrugations in phospholipid p beta, liquid crystals. *Biophysical journal*, 43(2):157–165, 1983. 44

[164] Vernita D Gordon, Paul A Beales, Gemma C Shearman, Zhijun Zhao, John M Seddon, Wilson CK Poon, and Stefan U Egelhaaf. Solid-like domains in mixed lipid bilayers: effect of membrane lamellarity and transition pathway. *Adv. Planar Lipid Bilayers Liposomes*, pages 137–153, 2014. 45

[165] Sung-Joo E Lee, Yuko Hori, and Arup K Chakraborty. Low t cell receptor expression and thermal fluctuations contribute to formation of dynamic multifocal synapses in thymocytes. *Proceedings of the National Academy of Sciences*, 100(8):4383–4388, 2003. 47

[166] Subhadip Raychaudhuri, Arup K Chakraborty, and Mehran Kardar. Effective membrane model of the immunological synapse. *Physical review letters*, 91(20):208101, 2003. 47, 49

[167] Thomas R Weikl and Reinhard Lipowsky. Pattern formation during t-cell adhesion. *Biophysical journal*, 87(6):3665–3678, 2004. 47, 49

[168] Michael L Dustin and Andrey S Shaw. Costimulation: building an immunological synapse. *Science*, 283(5402):649–650, 1999. 48

[169] Daniel Schmidt, Timo Bihr, Susanne Fenz, Rudolf Merkel, Udo Seifert, Kheya Sengupta, and Ana-Sunčana Smith. Crowding of receptors induces ring-like adhesions in model membranes. *Biochimica et Biophysica Acta (BBA)-Molecular Cell Research*, 1853(11):2984–2991, 2015. 49

[170] T Parasassi, G De Stasio, G Ravagnan, RM Rusch, and E Gratton. Quantitation of lipid phases in phospholipid vesicles by the generalized polarization of laurdan fluorescence. *Biophysical journal*, 60(1):179–189, 1991. 55

[171] Mohammad Abu Sayem Karal, Victor Levadnyy, and Masahito Yamazaki. Analysis of constant tension-induced rupture of lipid membranes using activation energy. *Physical Chemistry Chemical Physics*, 18(19):13487–13495, 2016. 57, 58, 65

[172] Evan Evans, Volkmar Heinrich, Florian Ludwig, and Wieslawa Rawicz. Dynamic tension spectroscopy and strength of biomembranes. *Biophysical journal*, 85(4):2342–2350, 2003. 58

[173] Olivier Sandre, Laurent Moreaux, and Françoise Brochard-Wyart. Dynamics of transient pores in stretched vesicles. *Proceedings of the National Academy of Sciences*, 96(19):10591–10596, 1999. 58, 65, 66

[174] Victor Levadny, Taka-aki Tsuboi, Marina Belaya, and Masahito Yamazaki. Rate constant of tension-induced pore formation in lipid membranes. *Langmuir*, 29(12):3848–3852, 2013. 58

[175] Mohammad Abu Sayem Karal and Masahito Yamazaki. Communication: Activation energy of tension-induced pore formation in lipid membranes, 2015. 60, 65

[176] Jérôme Solon, Pia Streicher, Ralf Richter, Françoise Brochard-Wyart, and Patricia Bassereau. Vesicles surfing on a lipid bilayer: Self-induced haptotactic motion. *Proceedings of the National Academy of Sciences*, 103(33):12382–12387, 2006. 66